# Distinct roles of cyclones and anticyclones in setting the midwinter minimum of the North Pacific eddy activity. Part I: Lagrangian perspective

Satoru Okajima,[a] Hisashi Nakamura,[a] Yohai Kaspi,[b]

[a] *Research Center for Advanced Science and Technology, The University of Tokyo, Tokyo, Japan*

[b] *Department of Earth and Planetary Sciences, Weizmann Institute of Science, Rehovot, Israel*



*Corresponding author*: Satoru Okajima, okajima@atmos.rcast.u-tokyo.ac.jp

## ABSTRACT

The North Pacific storm-track activity is suppressed substantially under the excessively strong westerlies to form a distinct minimum in midwinter, which seems inconsistent with linear baroclinic instability theory. This “midwinter minimum” of the storm-track activity has been intensively investigated for decades as a test case for the storm-track dynamics. However, the mechanisms controlling it are yet to be fully unveiled and are still under debate. Here we investigate the detailed seasonal evolution of the climatological density of surface migratory anticyclones over the North Pacific, in comparison with its counterpart for cyclones, based on a Lagrangian tracking algorithm. We demonstrate that the frequency of surface cyclones over the North Pacific maximizes in midwinter, whereas that of anticyclones exhibits a distinct midwinter minimum under the upstream influence, especially from the Japan Sea. In midwinter, it is only on such a rare occasion that prominent weakening of the East Asian winter monsoon allows a migratory anticyclone to form over the Japan Sea, despite the unfavorable climatological-mean conditions due to persistent monsoonal cold-air outbreaks and excessively strong upper-tropospheric westerlies. The midwinter minimum of the North Pacific anticyclone density suggests that anticyclones are the key to understanding the midwinter minimum of the North Pacific storm-track activity as measured by Eulerian eddy statistics.

## 1. Introduction

In midlatitudes, transient cyclones and anticyclones successively develop in travelling eastward, leaving stacks of their tracks, or often called "storm-tracks." Those transient disturbances not merely regulate day-to-day weather variations in the extratropics, but also interact with a background state to maintain the climatological-mean state such as the distinct midlatitude westerly jets, and the global atmospheric energy budget through transporting momentum and heat systematically.

Studies of such sub-weekly transient disturbances have arisen from the surveillance of the path and intensity of "storms." In the late 19th century, typical paths of storms were recognized reasonably in the Euro-Atlantic sector (Hinman 1888). Until the late 20th century, distribution of cyclone frequency has been examined based on surface weather charts (Klein 1958; Whittaker and Horn 1984), to reveal that cyclone frequency is particularly high over the North Pacific (NP) and North Atlantic (NA). With the development of atmospheric gridded data, procedures have been proposed to identify centers of cyclones and anticyclones more objectively (e.g., Parker et al. 1989; Bell and Bosart 1989; Murray and Simmonds 1991; Hodges 1994, 1995). Until today, many studies have utilized various tracking algorithms (Ulbrich et al. 2009; Neu et al. 2013). They identify and track centers of cyclones or anticyclones based typically on fields of sea-level pressure (SLP) or low-level vorticity. These "Lagrangian" tracking algorithms enable us to analyze individual transient eddies and associated phenomena, including winds, temperature, and precipitation. Based on identified low-level cyclonic centers, composited structures of cyclones have been constructed by using atmospheric reanalysis data (Manobianco 1989; Wang and Rogers 2001) and output of a general circulation model (GCM) experiment (Catto et al. 2010).

The development of another methodology for storm-track studies based on an "Eulerian" perspective lagged behind the Lagrangian method. Pioneering works such as Sawyer (1970) and Blackmon (1976) suggested that regions of particularly large band-pass-filtered fluctuations of 500-hPa height closely correspond to those of frequent cyclone paths over the NA and NP basins. Since then, (co-)variance of band-pass- or high-pass-filtered fluctuations has been commonly used as a local measure of activity of extratropical transient eddies (e.g., Blackmon et al. 1977, 1984; Chang et al. 2002; Nakamura et al. 2004).

According to the theory of baroclinic instability, stronger vertical shear of zonal winds is equivalent to larger maximum growth rate of eddies (Eady 1949). Consistently with this

principle, the NA storm-track activity is on average maximized in midwinter, when the climatological-mean upper-tropospheric westerly jet speed peaks. The corresponding NP storm-track activity, to the contrary, exhibits a distinct minimum in midwinter despite the maximum speed of the upper-tropospheric westerly jet (Nakamura 1992), which is apparently inconsistent with the baroclinic instability theory.

This distinctive seasonality is referred to as "midwinter minimum (MWM)" or "midwinter suppression" of the NP storm-track activity. It has long been investigated from various viewpoints as a "test case" for the midlatitude storm-track dynamics. The MWM of the NP storm-track is also simulated in numerical models. Zhang and Held (1999) successfully simulated the MWM in a stochastic linear storm-track model, implying that it is mainly caused by linear dry dynamics, although a similar effort by Whitaker and Sardeshmukh (1998) was not successful. The MWM is represented in a GCM (Christoph et al. 1997), and it is generally reproduced in the historical experiment with CMIP6 GCMs (Yang et al. 2021). Furthermore, Martian reanalysis datasets reveal transient eddy activity exhibits a minimum around winter solstice (*solstitial pause*; Lewis et al. 2016; Battalio 2022).

Since its discovery, multiple mechanisms have been proposed for the explanation of the MWM of the NP storm-track activity. Harnik and Chang (2004) as well as Deng and Mak (2005) pointed out the possible influence of the prominent lateral shear of the excessively strong midwinter jet on the suppressed growth rate of baroclinic eddies through "barotropic governor" effect, which is related to the results obtained by James (1987). As for the jet structure, the seasonal transition of the NP jet characteristics between stronger and more subtropical "merged" jet in midwinter and weaker eddy-driven "separate" jet in the shoulder seasons may be responsible for the MWM of the storm-track activity (Lachmy and Harnik 2014, 2016; Yuval et al. 2018; Yuval and Kaspi 2018). Using an idealized GCM with zonally symmetric setting, Novak et al. (2020) emphasized the importance of the climatological southward shift of the Pacific jet in midwinter. As supportive evidence for the importance of the strength of the jet, Afargan and Kaspi (2017) found a clear suppression of high-frequency eddy activity even over the NA in cases of the particularly strong NA jet in midwinter. Those cases were also characterized by the jet being anomalously equatorward. Nakamura (1992) and Nakamura et al. (2002) suggested that the baroclinic development of transient eddies may be inhibited under their excessive propagation speed owing to shortening the residence time

over the baroclinic zone. Nakamura and Sampe (2002) pointed out that upper-level eddies tend to be trapped into the equatorward- and upward-shifted "hybrid" NP jet core in midwinter and are therefore more likely to disconnected from the near-surface baroclinic zone, which is thus unfavorable for effective baroclinic growth of eddies. In addition, effect of diabatic heating associated with low-level clouds in the cold sector of surface cyclones was investigated by Chang (2001) and Chang and Song (2006). Park et al. (2010) and Lee et al. (2013) suggested the potential importance of large-scale orography.

Instead of taking a process-by-process approach, some studies have taken advantage of a framework of atmospheric energetics (Chang 2001; Zhao and Liang 2019; Schemm and Rivière 2019), which has evolved in the framework put forward by Lorenz (1955). Most recently, Okajima et al. (2022a) evaluated the detailed seasonal evolution of energy conversion/generation rates associated with transient eddies along the NP storm-track, in a normalized fashion by the eddy total energy. Their energetics was performed from a comprehensive perspective of the MWM of the NP storm-track activity that encompasses various mechanisms proposed by previous studies. They pointed out that the net normalized energy conversion/generation rate is indeed suppressed in midwinter. Specifically, EAPE conversion plays a substantial role especially in the reduction of the net normalized energy conversion/generation rate from its early-winter peak, whereas that of the net energy influx into the NP is of particular importance for the spring recovery.

The above studies are based basically on Eulerian eddy statistics. Studies of the MWM of the NP storm-track activity from the Lagrangian perspective have been relatively few. Penny et al. (2010) focused on the importance of upper-level cyclonic eddies propagating from the Asian continent upstream of the storm-track ("seeding effect"), through a Lagrangian tracking method. They suggested that a significant seasonal reduction of cyclonic eddies is responsible for the MWM, although no such clear relationship was found in an independent analysis by Chang and Guo (2012). Hoskins and Hodges (2019a, b) investigated seasonal evolution of the number and intensity of upper- and lower-tropospheric cyclones over the Northern Hemisphere. They demonstrated that, in the western NP, both the number and intensity of upper-tropospheric cyclones along the storm-track axis tend to minimize in midwinter, while the number of lower-tropospheric cyclones peaks in midwinter but their intensity exhibits a weak MWM. Schemm and Schneider (2018) examined the relationship among storm-track activity, number, and lifetime of surface cyclones over the NP. They

suggested that shorter lifetime of cyclones in midwinter may contribute to the MWM of the Eulerian storm-track activity. Subsequently, Schemm et al. (2021) suggested that cyclones downstream of Kamchatka are less numerous and less intense in January, contributing primarily to the MWM of the NP storm-track activity, along with a contribution from cyclones moving from the East China Sea (ECS) to the spring recovery of the NP storm-track activity. Most recently, through tracking of upper- and lower-tropospheric cyclonic eddies in idealized GCM simulations in which the jet strength was systematically increased, Hadas and Kaspi (2021) investigated the dependence of the number, intensity, and lifetime of those eddies on the jet intensity. As the jet strengthens and the corresponding vertical shear increases in the model, they found a tendency that the eddy coupling between the upper and lower levels diminishes, their westward-tilting baroclinic structure becomes broken and thus their baroclinic growth becomes suppressed. This tendency therefore results in an inverse relation between jet intensity and eddy growth under the excessively strong jet.

One of the major difficulties in understanding the MWM is a gap between the "Lagrangian" statistics of moving cyclones and "Eulerian" eddy statistics that depict the MWM of the NP storm-track activity. The latter regards transient eddies as waves where contributions from both cyclonic and anticyclonic deviations are combined (Wallace et al. 1988). Meanwhile, those studies of the MWM from the Lagrangian perspective focus mainly on cyclones, while excluding the potential contribution from anticyclones, which makes it difficult to compare quantitatively the results obtained from the two different perspectives. Of course, there is no necessity for measures of eddy activity from the Lagrangian and Eulerian perspectives to accord with one another. In Schemm and Schneider (2018), for instance, distributions of the Lagrangian surface cyclone density and Eulerian eddy activity differ substantially; the former is highest over the Gulf of Alaska, whereas the latter maximizes along a zonal band at ~40°N. A similar difference is also shown by Shaw et al. (2016).

With more attention paid to extratropical cyclones that are directly related to stormy weather, few studies have focused on the climatological-mean behavior of migratory anticyclones based on a tracking, especially over the NP. Hoskins and Hodges (2002) found that climatological wintertime distributions of cyclone and anticyclone densities distinctively differ over the NP. Specifically, the former is highest to the east of Japan, while the latter peaks along ~30°N. Since then, some studies have conducted a feature-tracking analysis for migratory anticyclones over the NP (Favre and Gershunov 2006; Iaonnidou and Yau 2008;

Kravtsov et al. 2015; Pepler et al. 2019), but they did not focus on the relationship between anticyclone tracks and storm-track activity measured as Eulerian eddy statistics. All in all, the role of migratory anticyclones in the formation of the "NP storm-track" within the Eulerian framework is still not well understood.

Recently, Okajima et al. (2021; hereafter cited as ONK21) have developed a method to separate cyclonic and anticyclonic contributions to Eulerian eddy statistics. They revealed that anticyclonic vortices play an important role in maintaining the midwinter Pacific jet, especially in the upper troposphere, and they make greater contributions to the barotropic energy conversion and net energy outflow for the midwinter NP storm-track. Their results therefore suggest that anticyclones should not be dismissed in investigating the MWM of the NP storm-track from the Lagrangian perspective.

To this end, the present study aims to investigate the detailed seasonal evolution of climatological density of surface migratory anticyclones over the NP, in comparison with that of cyclones, based on a Lagrangian tracking algorithm. We demonstrate that the seasonality of the frequency of surface anticyclones is substantially contributed by the upstream influence from the Japan Sea region and thus differs distinctively from that of cyclones. In a companion paper (Okajima et al. 2022b; hereafter Part II), seasonal evolution of the contributions from cyclonic and anticyclonic vortices to Eulerian eddy statistics are investigated.

This paper (Part I) is organized as follows; in section 2, data and analysis methods used in this study are explained. In section 3, seasonal evolution of climatological-mean activity of NP cyclones and anticyclones is described. Then, composite analysis is conducted to investigate mechanisms for the seasonality in section 4. Long-term modulations of the densities of cyclone and anticyclone centers are examined in section 5. Section 6 offers a summary and discussions.

## 2. Data and analysis methods

*a. observational data*

This study utilizes 6-hourly fields of atmospheric variables, including geopotential height, temperature, and wind velocities in pressure coordinates as well as sea-level pressure (SLP), taken from the Japanese 55-year reanalysis (JRA-55) by the Japan Meteorological Agency

(JMA) (Kobayashi et al. 2015; Harada et al. 2016) for the period 1958-2017. The JRA-55 has been constructed with a four-dimensional variational data assimilation (4D-Var) system with TL319 horizontal resolution (equivalent to 55-km resolution) and 60 vertical levels up to the 0.1-hPa level. Those variables are available on a 1.25°×1.25° grid.

At each grid point, sub-weekly fluctuations associated with synoptic-scale transient eddies have been extracted from the 6-hourly atmospheric reanalysis through an 8-day cutoff Lanczos filter with a 121-point window. Their low-frequency modulations have then been calculated locally as low-pass-filtered fields of their products, to represent eddy activity of fluxes. Climatological-mean fields are calculated with a 31-day running mean.

*b. Identification of tracks of surface migratory cyclones and anticyclones*

In this study, tracks of migratory cyclones and anticyclones are objectively identified based on the JRA-55 reanalysis, by identifying cyclones and anticyclones on a surface weather map, taking the different typical characteristics of cyclones and anticyclones into account. Assessment of the performance of the tracking algorithm is provided in the Appendix. We have also confirmed the robustness of tracking results with ~6000-years of a large ensemble GCM experiment (Supplementary Figs. S1 and S2).

1) CYCLONE TRACKS

For identifying surface cyclone centers, we adopt a tracking algorithm used in Kuwano-Yoshida et al. (2022). SLP and the Laplacian of SLP (hereafter, $\nabla^2$SLP) are utilized to identify cyclones on a surface weather map. The combination of SLP and $\nabla^2$SLP (or surface vorticity) has been adopted to identify cyclone tracks in previous studies (e.g., Murray and Simmonds 1991; Pinto et al. 2005; Simmonds et al. 2008; Hewson and Titley 2010). Before initiating the tracking, a Gaussian spatial filter whose half-amplitude length is 300km was applied to $\nabla^2$SLP to obtain a smoother field. Those grid points at which surface elevations are higher than 1500m were not used for the tracking to avoid identifying spurious centers.

First, local minima of SLP were regarded as candidates for cyclone centers, and among them only the SLP minimum with the lowest pressure in the vicinity of a 400km circle has been identified. The SLP minimum must accompany a local maximum of $\nabla^2$SLP within 700km, which must be stronger than 80 Pa/(100km)$^2$. This condition was imposed to discard weak cyclones with no significant amplitudes.

Next, those SLP minima identified above were compiled as tracks. Specifically, the nearest SLP minima at successive time steps were connected, only when the distance is not more than 800km. Any track must persist at least over 4 time-steps (viz. 24 hours) and must travel at least over 600km during the lifetime. A cyclone track must pass through a domain encompassing the NP storm-track [100°E−120°W, 20−65°N].

2) ANTICYCLONE TRACKS

For anticyclones, only SLP was used to identify their centers as in previous studies (Hoskins and Hodges 2002; Kravstov et al. 2015). Unlike cyclones, anticyclones are unlikely to have distinct $\nabla^2$SLP minima, reflecting the gradient wind balance. Local SLP maxima were regarded as candidates for anticyclone centers, after SLP has been horizontally smoothed with performing a 9-point horizontal smoothing (weight is 0.5 next to the center point and 0.3 at corners) eight times. Here, only a SLP maximum that is highest within a 400km circle around the maximum was identified as a surface anticyclonic center at which SLP should not be lower than 990 hPa.

Similar to the case for cyclone centers, the nearest SLP maxima identified above at successive time steps were connected. The distance must not exceed 1000km. Again, any track must persist at least over 4 time-steps (i.e., 24 hours) and travel at least over 600km during the lifetime. The distribution of their density is similar if longer thresholds for movement are imposed. Any anticyclone track must pass through the domain [100°−120°W, 20−65°N] around the NP storm-track.

## 3. Climatological-mean activity of North Pacific cyclones and anticyclones

Figure 1 shows horizontal distributions of climatological-mean densities of cyclone and anticyclone centers[1] from November to March. As shown in previous studies, the cyclone

[1] We are aware that density of those centers is affected by both the number of tracks and their lifetime. The present study focuses on density, because it can be compared with Eulerian eddy statistics in a more straightforward manner than the number of tracks, as well as it

246 density is high over the NP poleward of 30-35°N, in association with the climatological-mean
247 Aleutian Low (AL). Those cyclones tend to move eastward or northeastward (not shown).
248 Around the AL center, density of migratory cyclones maximizes in midwinter (Fig. 1b). Just
249 off the east coast of Japan at ~35°N, a hint of a local maximum of the cyclone density
250 suggests the influence from the Kuroshio Extension (KE) on the development of synoptic-
251 and meso-α-scale cyclones (Masunaga et al. 2020), especially from midwinter to early spring.
252 Another noticeable feature is high density along the south coast of Japan in spring (Fig. 1c),
253 corresponding to frequent “southern coast cyclones” around Japan (Takano 2002).

bypasses the potential uncertainty owing to splitting of tracks. Nevertheless, the influence by the number and duration is discussed in section 6.

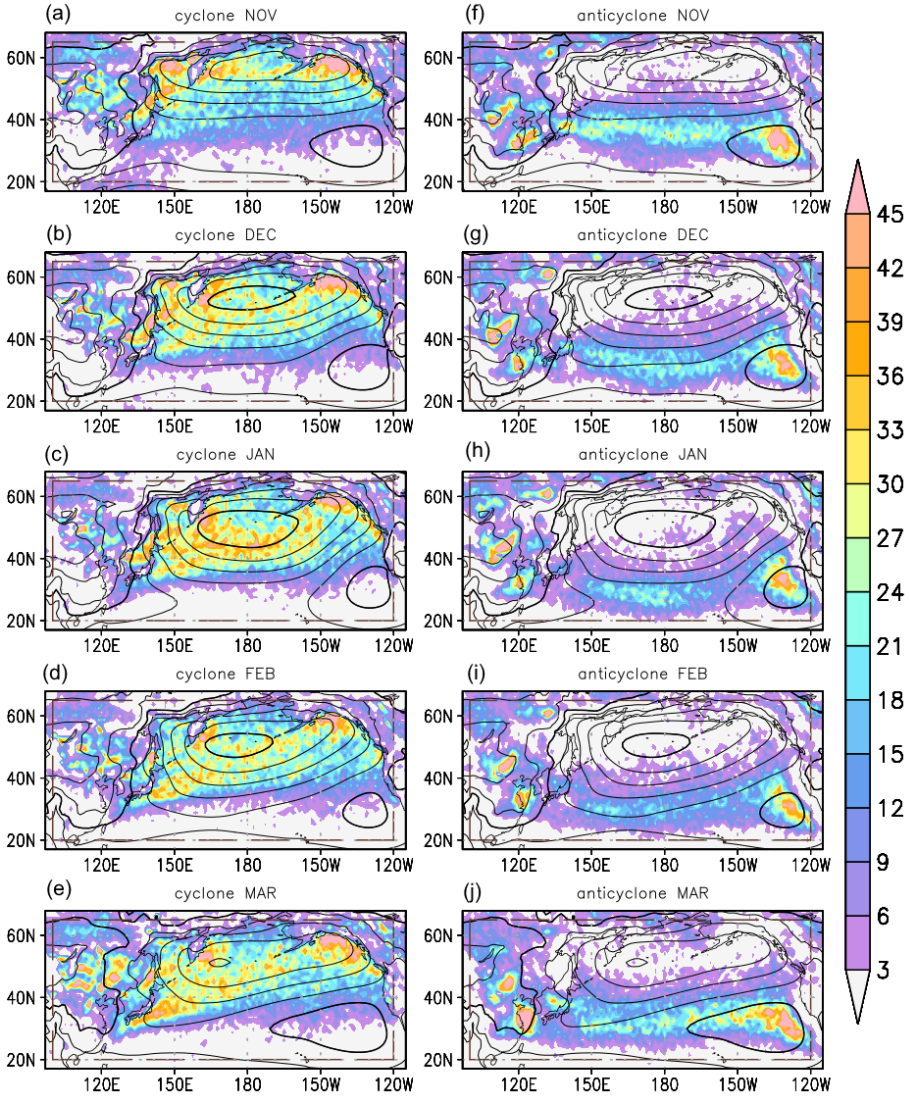


Fig. 1. Climatological-mean densities (*0.01%) of identified surface (a-e) cyclone and (f-j) anticyclone centers for the calendar months as indicated, based on 6-hourly SLP fields of the JRA-55 in 1958/59-2016/17. Meridians of 100°E and 120°W, and latitude circles of 20°N and 65°N are highlighted, which indicate the lateral boundaries of the domain through which those centers must pass. Contours indicate climatological-mean SLP (every 4hPa, thick for every 20hPa).

Conversely, the anticyclone density exhibits a zonally-extended band of maxima at ~30°N, slightly poleward of the climatological-mean subtropical high-pressure belt. Migratory anticyclones over the western and central NP tend to move eastward or southeastward especially in midwinter (not shown). The different moving directions between cyclones and anticyclones is consistent with previous studies (Wallace et al. 1988; Tamarin and Kaspi 2016). The maximum over the eastern NP collocates with the climatological-mean center of the subtropical high (Nakamura et al. 2010), which is consistent with Pepler et al. (2019). The density is also high over the Yellow Sea in addition to eastern and northern

China, which may correspond to synoptic-scale anticyclones that are separated from the persistent Siberian High. The anticyclone density in the storm-track entrance region (at ~140°E, 40°N) is reduced in midwinter compared with that in the shoulder seasons.

To highlight the seasonality of the cyclonic and anticyclonic densities in the NP storm-track core region, their latitude-season sections as zonal means for 150°−180E° are shown in Fig. 2. Cyclone density maximizes in midwinter, coincided with the climatological peak of the AL (Fig. 2a). The seasonality is consistent with Hoskins and Hodges (2019b). The region of highest cyclone density extends most southward in midwinter, leading to its striking midwinter maximum between 40°N and 50°N. Meanwhile, the latitude of maximum anticyclonic density migrates southward from 35°−40°N in the shoulder seasons to ~30°N in midwinter along with the subtropical high-pressure belt (Fig. 2b). In sharp contrast to the cyclonic density, the anticyclonic density shows its distinct MWM.

The contrasting seasonality between surface cyclone and anticyclone densities has not been described in previous studies. One may consider that the midwinter maximum of cyclone density may be compatible with the stronger westerly jet and baroclinicity in midwinter than in the shoulder seasons, leading to higher maximum growth rate of baroclinic eddies, which may also influence their intensity and lifetime. At the same time, however, the seasonality of NP cyclones suggests that it may not be responsible for the MWM of the NP storm-track activity as measured by Eulerian statistics. The contrasting seasonality suggests that migratory anticyclones can be of certain importance for the MWM of the NP storm-track activity.

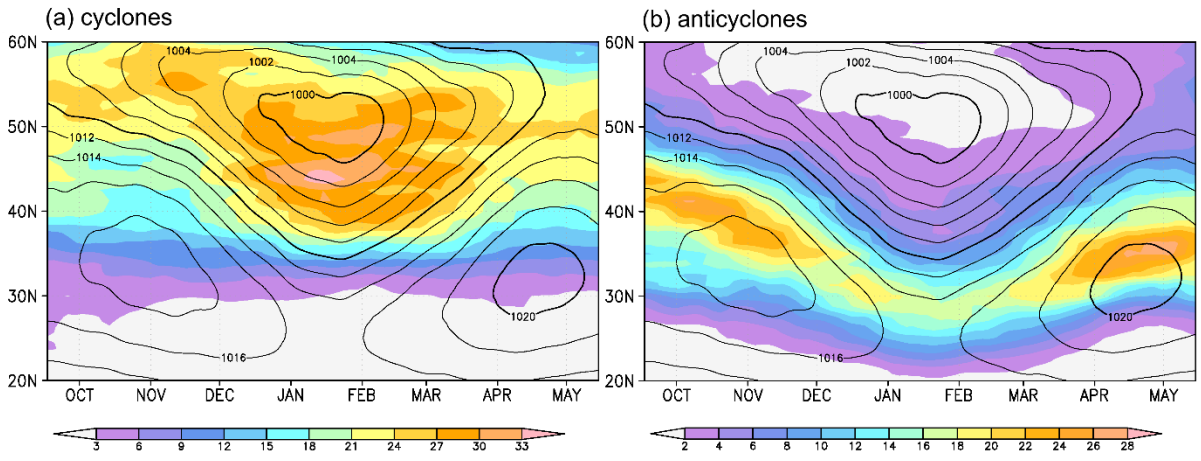


Fig. 2. Latitude-season sections of climatological-mean densities (*0.01%) of surface (a) cyclone and (b) anticyclone centers identified over the central NP based on 6-hourly SLP fields of the JRA-55 for 1958/59-2016/17. Contours indicate climatological-mean SLP (every

2 hPa, thick for every 10 hPa). All the quantities are longitudinally averaged between 150°E and 160°W. Labels on the ordinate mark the beginnings of the individual calendar months.

To delineate the striking difference in the seasonality between cyclone and anticyclone densities, only tracks passing the central NP domain [150°E−150°W, 20−65°N] are counted to illustrate where cyclones and anticyclones detected within the storm-track core region come from. The three calendar days in Fig. 3 correspond to the first peak, MWM, and the second peak during the seasonal cycle of the NP storm-track activity, especially for lower-tropospheric Eulerian eddy statistics (Okajima et al. 2022a). The NP cyclones tend to propagate from the northern Japan Sea and the Okhotsk Sea in early winter (Fig. 3a), whereas in spring more cyclones tend to travel along the Kuroshio just south of Japan and then along the KE (Fig. 3c). Propagation from the ECS is also more frequent in spring. These cyclone paths seem to correspond to the two branches of the upper-level disturbances pointed out by Chang (2005), and they are also consistent with Schemm et al. (2021). Another noticeable aspect is that the number of cyclones propagating from northern China (especially west of 120°E) decreases in midwinter (Fig. 3b), suggestive of reduced cyclone activity along ~50°N over East Asia, and consistent with the upstream "seeding" effect pointed out by Penny et al. (2010).

The NP anticyclones are likely to propagate from the Japan Sea in early winter and spring (Figs. 3d and 3f). This typical pathway is consistent with the climatologies for SON, DJF, and MAM obtained by Pepler et al. (2019). The propagation is greatly suppressed in midwinter (Fig. 3e), suggestive of the important contribution of anticyclones traveling from the Japan Sea for the NP anticyclone density. The high density around the Yellow Sea may be due to rather slow movement of anticyclones (not shown) after separated from the SH, as hinted by climatological SLP contours (Fig. 3f).

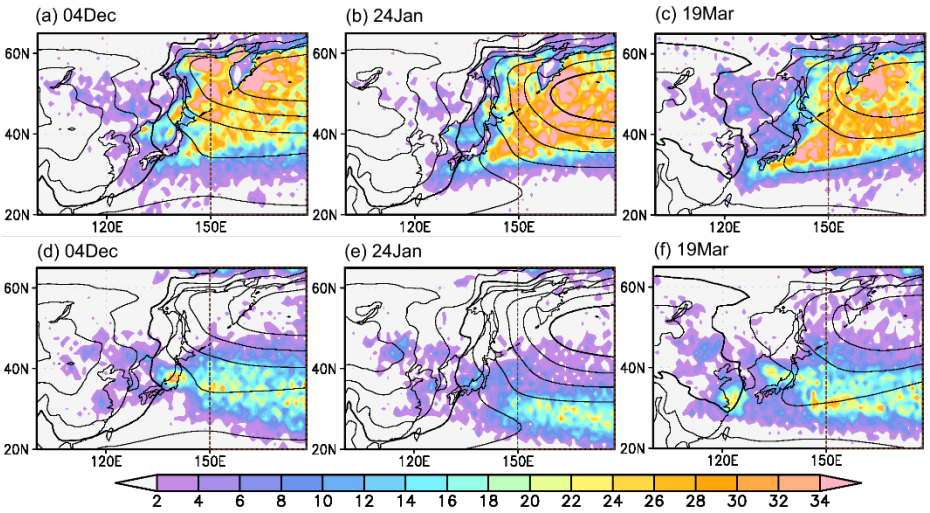


Fig. 3. Same as in Fig. 1, but for identified surface (a-c) cyclone and (d-f) anticyclone centers passing through the domain [150°−150°W, 20°−65°N] over the central NP as climatologies for the calendar days as indicated.

To further investigate the origin of the NP cyclones and anticyclones, frequency of their geneses is shown in Fig. 4. Cyclogenesis occurs most frequently over the KE and around the Kamchatka Peninsula. The latter signifies cyclones generated locally around the peninsula, and the number of these cyclones decreases in spring, when cyclogenesis over ECS becomes more frequent (Fig. 4c). These results are consistent with Schemm et al. (2021), and the frequent midwinter cyclogenesis over the KE is in agreement with Masunaga et al. (2020). Conversely, genesis of anticyclones is most likely around Japan. In early winter and midwinter, genesis is most frequent over the central Japan Sea (Figs. 4d and 4e). In spring (Fig. 4f), genesis around Japan becomes less frequent, implying that the high anticyclone density over the Japan Sea in Fig. 3f is due to genesis around the northwestern Japan Sea or farther upstream over China (west of 120°E).

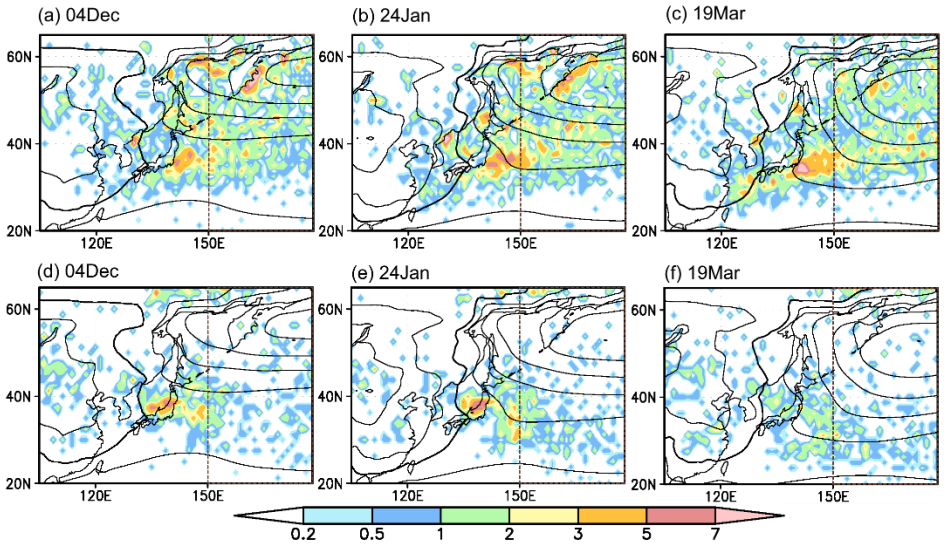


Fig. 4. (a-c) Climatological-mean density (*0.01%) of the genesis of surface cyclones that pass through the domain [150°−150°W, 20°−65°N] over the central NP, for the calendar days as indicated. Black contours denote climatological-mean SLP (every 4hPa). (d-f) Same as in (a-c), respectively, but for the genesis of identified anticyclones.

The results obtained thus far suggest that anticyclones around the Japan Sea can be important for the seasonality of anticyclone density over the NP. To assess the influence on the NP storm-track activity from upstream, the densities of cyclones and anticyclones shown in Fig. 2 for the NP are decomposed into those due to those cyclones and anticyclones that have passed through the domain [130°−140°E, 35°−42°N] over the Japan Sea (JPS) and the residuals (Fig. 5). As evident in Fig. 5b, the dual peaks of the NP anticyclone density in autumn and spring as well as its distinct MWM are explained exclusively by anticyclones coming from upstream. This can be confirmed also by the nearly constant density of the residual anticyclones throughout the cold season (Fig. 5d). Conversely, cyclones coming from the JPS domain exert only modest influence on the seasonality in the NP cyclone density in Fig. 2a compared to the residual (Figs. 5a and 5c). Although migratory cyclones are more numerous from early- to mid-winter along ~41°N over the JPS domain (not shown), a substantial fraction of those cyclones must be meso-α-scale cyclones that develop within monsoonal cold airflows associated with upper-level cold cyclonic vortices, which are most frequent in January (Yanase et al. 2016; Watanabe et al. 2018).

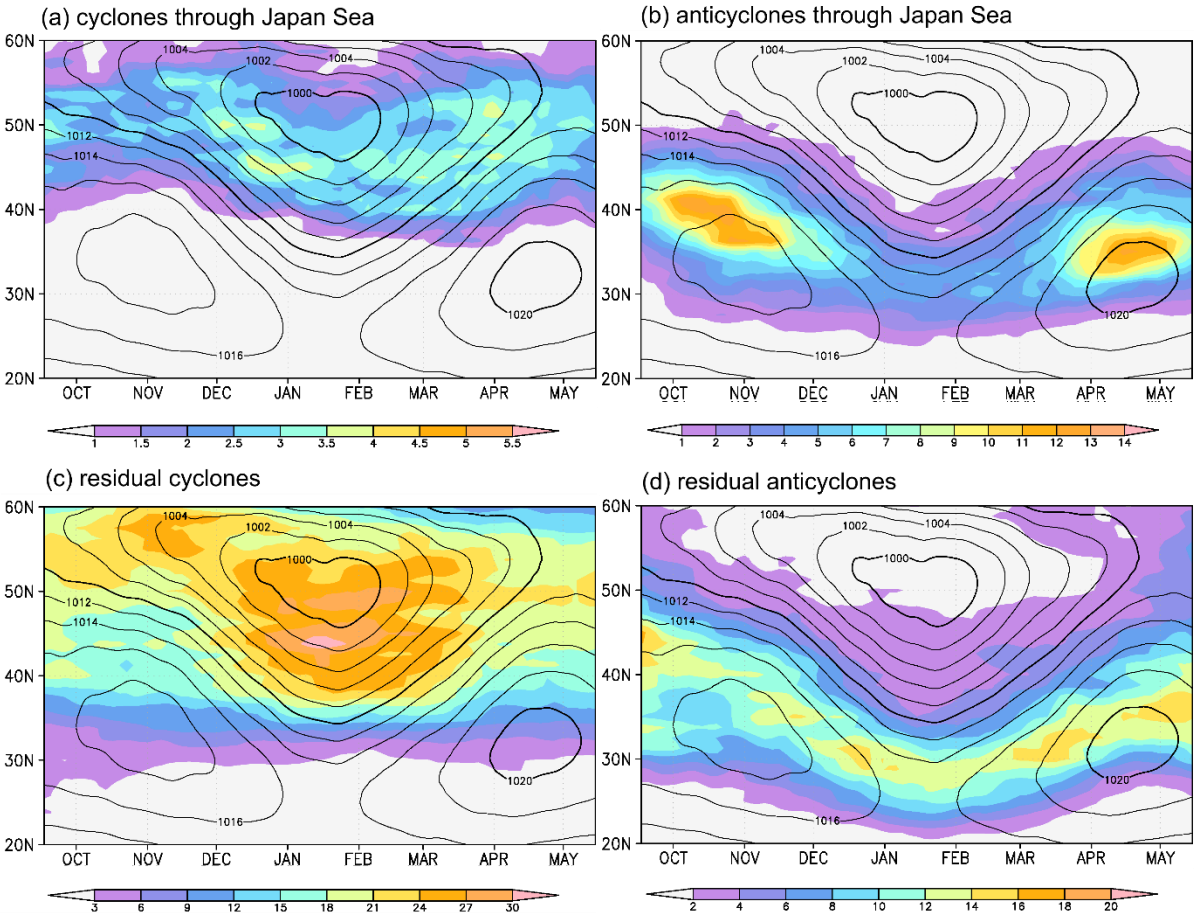


Fig. 5. (a, b) Same as in Figs. 2a-b, respectively, but for identified cyclones and anticyclones that pass through the domain [130°−140°E, 35°−42°N] over the Japan Sea (JPS) during their lifetimes. (c, d) Same as in (a-b), respectively, but for cyclones and anticyclones that *do not* pass through the JPS domain during their lifetimes.

Activity of synoptic-scale disturbances is strongly influenced by upper-tropospheric eddies (Takayabu 1991). To examine the seasonality of upper-level eddy activity, frequencies of cyclonic and anticyclonic vortices are evaluated by a method based on local curvature introduced by ONK21. The curvature thresholds are set to be $\pm 4\times10^{-7}$ $m^{-1}$ for cyclonic and anticyclonic vortices, respectively, which correspond to circulation of radius less than 2500 km. Note that this method is unlikely to be influenced strongly by the actual size of an individual migratory trough or ridge, because their radii must be smaller than 2500 km. Nevertheless, the result is qualitatively similar when centers of vortices (equivalently, local extrema of curvature) are tracked in an analogous manner to the surface tracking algorithm (See Supplementary Fig. S3). The result is also qualitatively similar with a threshold radius of 1000km.

Both in the western NP (Fig. 6a) and JPS (Fig. 6c) sectors, cyclonic vortices are less frequent around the axis of the upper-tropospheric westerly jet-stream and its southern flank than to the north, in good agreement with ONK21. The probability of upper-level cyclonic vortices peaks in midwinter at ~45°N and to the north, where the surface cyclone density also maximizes over the central NP (Fig. 2a). This is also consistent with Watanabe et al. (2018), who showed that a surface meso-α-scale cyclone in midwinter over the Japan Sea tends to be accompanied by an intense free-tropospheric pressure trough. Conversely, upper-level anticyclonic vortices tend to be less frequent in the extratropical western NP (Figs. 6b and 6d), except along the southern flank of the jet-stream in autumn and spring. The MWM of frequency of anticyclonic vortices is evident over both the NP and JPS sectors, which is consistent with the suppressed activity of surface anticyclones.

The result showing the midwinter maximum of the frequency of upper-tropospheric cyclonic vortices over the JPS sector may apparently be inconsistent with Penny et al. (2010), who showed that the "seeding effect" on the NP storm-track from the upstream is less effective in midwinter than in the shoulder seasons, based on a tracking of negative anomalies of high-pass-filtered 300-hPa height. Actually, our 300-hPa curvature tracking applied to a sector west of 130°E indicates that the frequency of cyclonic vortices does not maximize in midwinter but rather it is slightly reduced between the peaks in the shoulder seasons north of ~40°N (not shown). Together with the MWM in frequency of cyclonic vortices over the Eurasian continent south of 40°N, the seasonality revealed by our analysis is compatible with Penny et al. (2010).

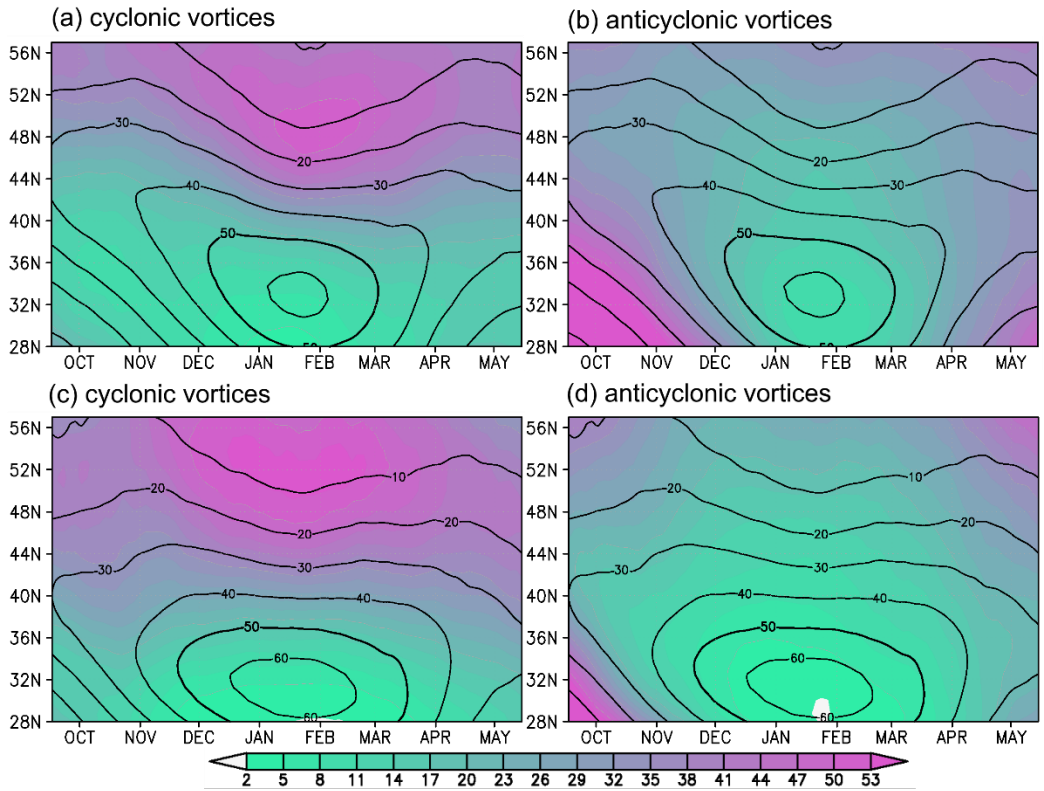


Fig. 6. Latitude-season sections of climatological-mean probability (colors, %) of domains of (a) cyclonic and (b) anticyclonic vortices at 300-hPa based on curvature. Grid points where instantaneous curvature radius is smaller than 2500 km are counted as domains of cyclonic or anticyclonic vortices depending on their sign. Contours indicate climatological-mean $U_{300}$ (every 10 m/s). All the quantities plotted are averaged zonally between 150°E and 180°. (c, d) Same as in (a, b), respectively, but for probability averaged between 130°E and 140°E.

## 4. Composite analysis for anticyclones over the Japan Sea

In section 3, we have demonstrated that anticyclones from the JPS sector is of critical importance for the seasonality of anticyclone density over the NP. To elucidate the structure and associated environment for those anticyclones, Figs. 7a-c show a composited three-dimensional structure of those anticyclones moving over the JPS sector after shifting their surface centers horizontally in such a manner that they are collected at the origin of coordinates. The composited SLP fields (Figs. 7a-c) suggest features of a synoptic-scale anticyclone separated from the climatological-mean Siberian High (SH). The typical vertical structure of the composited anticyclonic anomalies over the JPS region is shown in Figs. 7d-f, as latitudinal averages of high-pass-filtered geopotential height and temperature from 10° south to 10° north of the composited centers. Those figures highlight westward-tilted height anomalies with altitude, showing their baroclinic nature. The midwinter JPS surface

anticyclones tend to be accompanied by stronger upper-tropospheric height anomalies (Fig. 7e) than their counterpart in the shoulder seasons (Figs. 7d and 7f), which is not the case for surface cyclones over the JPS (not shown).

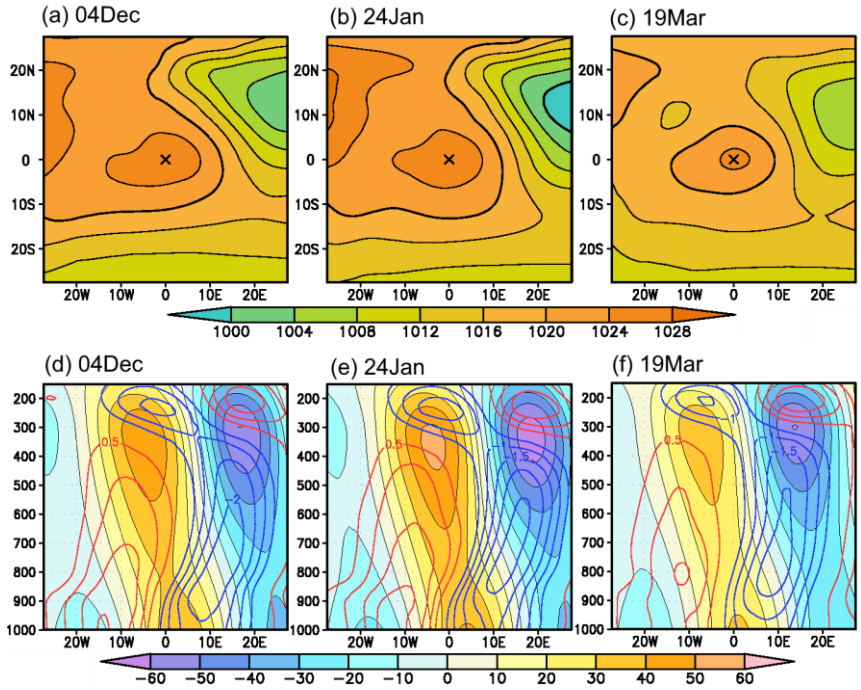


Fig. 7. (a-c) Composited fields of SLP (hPa) based on the surface anticyclone centers identified for the calendar days as indicated. Before the compositing, all selected SLP fields have been shifted horizontally in such a manner that the surface anticyclone centers are collocated at a grid point as indicated in each of the panels and marked with a black cross. Labels on the abscissa and ordinated denote longitudes and latitudes (in degree) relative to the center. (d-f) Zonal sections of the composited high-pass-filtered anomalies in geopotential height (colors, m) and temperature (colored contours, K) for the surface anticyclones for the indicated calendar days. In each panel, variables are averaged over a 20° latitudinal band centered at the latitude of an identified surface anticyclone center.

A question arising here is what kind of background field is favorable for an anticyclone to exist over the JPS. When we calculate a composited SLP field at time steps when a surface anticyclone is located over the midwinter JPS, SLP over the Asian continent is lower than the climatology (not shown), indicative of the weakened SH. To investigate an anomalous background state for a JPS anticyclone, we composite a low-pass-filtered anomaly field of a given variable $X$ defined as $[X]_L \equiv [X] - [X]' - X_C$, where $[X]$ denotes a composited field, prime high-pass-filtered field, and subscript $c$ the climatological mean. Figure 8 shows $[Z_{300}]_L$ and $[T_{850}]_L$ when an anticyclone exists over the JPS domain. An anticyclonic $[Z_{300}]_L$ anomaly spreads over midlatitude East Asia (Fig. 8b), suggesting the weakened climatological-mean East Asian trough. The corresponding warm anomaly over East Asia

indicates that the East Asian cold monsoonal airflow is weaker associated with a surface JPS anticyclone (Fig. 8e). Furthermore, those low-frequency anomalies are strongest in midwinter (Fig. 8). These results indicate that the marked weakening of the climatological-mean East Asian trough and monsoonal cold surge is needed in midwinter for a surface anticyclone to be cut off from the SH into the JPS sector. This seasonality implies that migratory anticyclones over the JPS sector are more unlikely in midwinter under seasonally-enhanced cold surge from the SH.

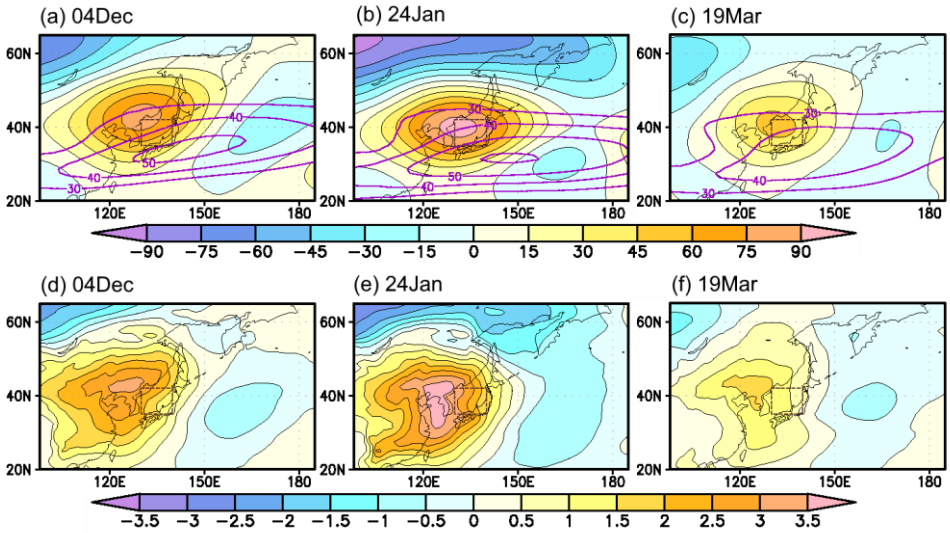


Fig. 8. (a-c) Composite maps of low-frequency anomalies of 300-hPa geopotential height (colors, m) at time steps when one or more anticyclonic centers are located over the Japan Sea domain [130°−140°E, 35°−42°N; indicated with dashed rectangles] for the calendar days as indicated. Purple contours indicate composited low-frequency component of $U_{300}$ (m/s). (d-f) Same as in (a-c), respectively, but for low-frequency anomalies of temperature at 850-hPa (K).

To investigate upstream influence on the low-frequency height anomaly over midlatitude East Asia, a wave-activity flux defined by Takaya and Nakamura (2001) is utilized. The low-frequency anticyclonic anomaly in the upper troposphere is influenced by wave-activity injection from the upstream (Figs. 9a-c). Wave-activity flux extends over Siberia through a cyclonic anomaly at ~100°E especially in midwinter. These cyclonic and anticyclonic anomalies are quasi-stationary and roughly along the polar-front jet, as seen in lag-composite maps by three days especially in early- to midwinter (Figs. 9d-f). The wavetrain resembles the Eurasian teleconnection (EU) pattern (Wallace and Gutzler 1981), which is one of the dominant teleconnection patterns in the wintertime Northern Hemisphere. Actually, the wavetrain shown in Fig. 9e resembles the composite map at lag −3 days based on the EU

pattern index (Wang and Zhang, 2015). The wavetrain also resembles the Scandinavian pattern in January (Bueh and Nakamura 2007). In addition, a similar wavetrain but with the reversed polarity is observed in blocking events around [57°N, 80°E] in association with the intensified surface SH (Takaya and Nakamura 2005), suggesting the potential influence by upstream blocking events and North Atlantic.

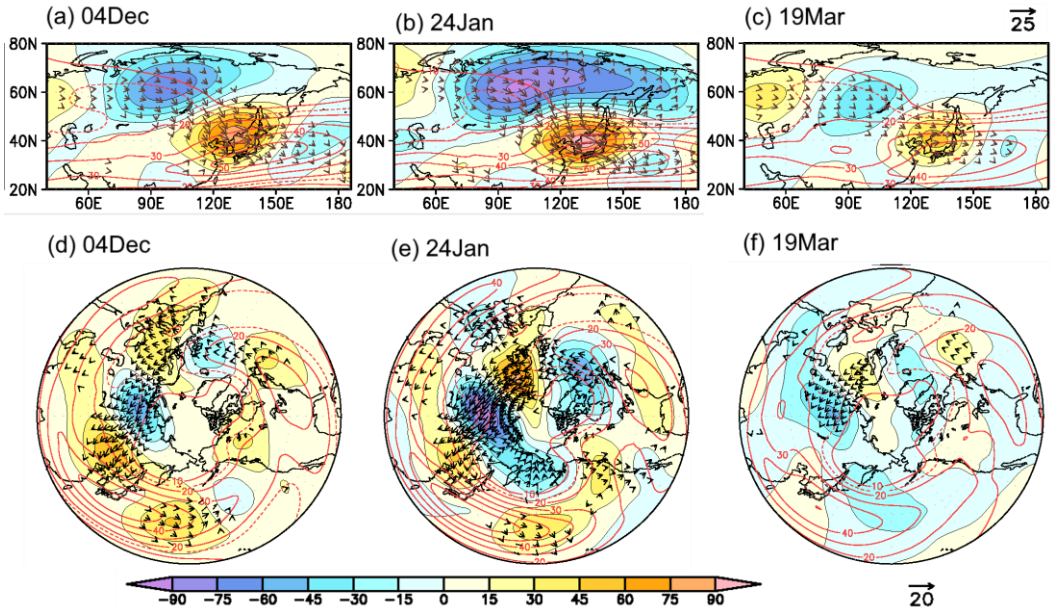


Fig. 9. (a-c) Composite map of low-frequency anomalies of 300-hPa geopotential height (colors, m) at time steps when one or more anticyclonic centers are located over the Japan Sea domain (indicated with dashed rectangles) for the calendar days as indicated. Vectors indicate a Rossby wave-activity flux ($m^2/s^2$) at 300-hPa defined by Takaya and Nakamura (2001). (d-f) Same as in (a-c), respectively, but for time steps leading those in (a-c) by 3 days.

To investigate the vertical structure of the low-frequency anomalies associated with JPS surface anticyclones, meridional sections are constructed by taking a zonal average between 130°E and 140°E. As evident in Figs. 10a-c, the low-frequency anomalies are characterized by dipolar anomalies in upper-level zonal winds. The westerlies are anomalously weakened around the jet core and enhanced to its north, representing a poleward widening of the jet. These low-frequency anomalies associated with the JPS surface anticyclones are strongest in midwinter (Fig. 10b), rendering the jet structure in midwinter similar to its counterpart as often observed in the shoulder seasons (Figs. 10a and 10c). Consistently, the dipolar upper-level wind anomalies accompany a warm anomaly over the JPS throughout the depth of the troposphere, capped by a cool anomaly at the tropopause level (Figs. 10d-f). Again, these thermal anomalies are maximized in midwinter. Associated with these anomalies, static stability is lowered by ~20% and thus the Rossby depth ($\equiv fL/N$, with horizontal scale $L$ and

the Brunt-Väisälä frequency *N*) increases, especially in the mid-troposphere. Due to the combined effects of the lowered static stability and the reduced jet intensity in midwinter that can weaken the trapping effect of upper-level eddies into the jet core, upper-tropospheric eddies tend to be linked more strongly with the lower-tropospheric anomalies for their baroclinic development.

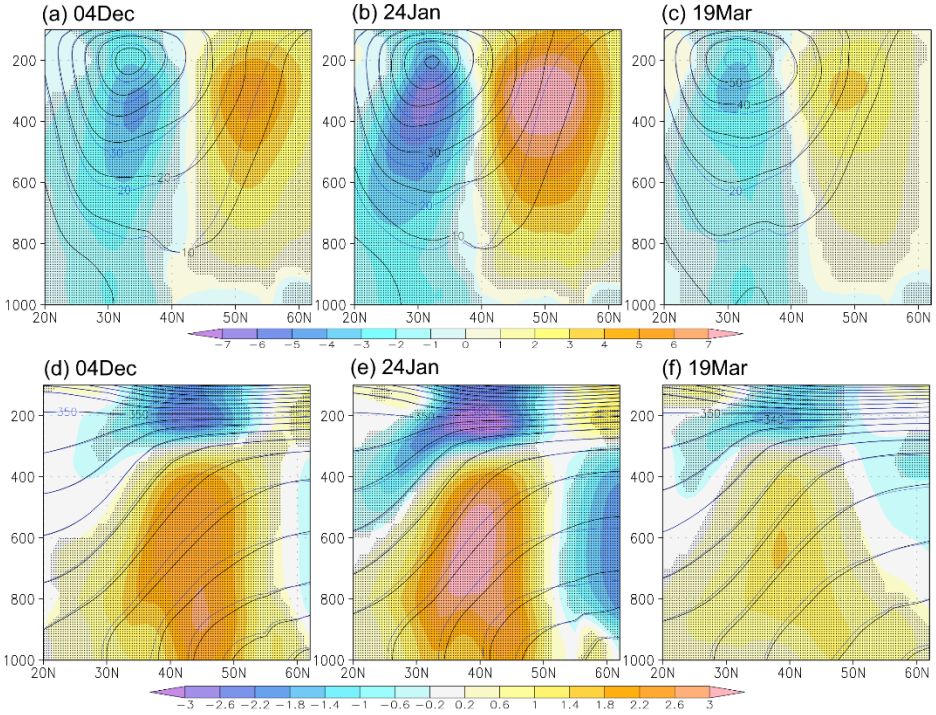


Fig. 10. (a-c) Meridional sections of composited low-frequency anomalies of westerly wind speed (colors, m/s) at time steps when one or more anticyclonic centers are located over the Japan Sea domain for the calendar days as indicated. Black and blue contours indicate composited low-frequency component and climatological-mean of westerly wind speed, respectively (every 10m/s). All the quantities plotted have been averaged between 130°E and 140°E. Stippling indicates statistically significant difference at the 95% confidence level based on a random subsampling of time steps by 5000 times, the number of which is the same as that of cyclones used for respective composites (viz. 176, 114, and 226), within the entire time steps used for 31-day running-mean climatologies around the respective calendar days of individual years (i.e., 31*4*59). (d-f) Same as in (a-c), respectively, but for low-frequency anomalies of potential temperature (colors, K). Black and blue contours indicate composited low-frequency component and climatological-mean potential temperature, respectively (every 10K).

As the midwinter climatology (Fig. 11b), vertical gradient of potential temperature, corresponding to static stability, is pronounced at the tropopause level to the north of the jet core, while it is relatively low in the free troposphere over the JPS sector and much lower near the surface. Compared with the midwinter situation, static stability tends to be slightly lower in the mid- and upper troposphere in the shoulder seasons (Figs. 11a and 11c),

514 suggesting the climatologically greater Rossby depth. The midwinter maximum of mid-
515 tropospheric static stability, which seems consistent with the result obtained by Frierson and
516 Davis (2011) from a zonal-mean perspective, probably reflects seasonally enhanced cold
517 surge from the stronger SH (Zhang et al. 1997). The smaller Rossby depth retards the vertical
518 connection of upper-tropospheric eddies with lower-tropospheric eddies, which can
519 contribute to less frequent surface anticyclones over JPS together with fewer upper-
520 tropospheric anticyclonic vortices. The discussion is consistent with the tendency for upper-
521 tropospheric eddies to be trapped in the jet core and thus less connected with the surface
522 baroclinic zone anchored by the midlatitude oceanic frontal zone, as argued by Nakamura and
523 Sampe (2002). In addition, excessively strong vertical shear of the westerlies in midwinter
524 (namely, small Richardson number) may render the vertical scale of eddies smaller than the
525 corresponding Rossby depth, as indicated as a characteristic of non-geostrophic baroclinic
526 instability by Nakamura (1988). The retarded vertical linkage of upper-tropospheric vortices
527 with surface anticyclones can be seen in the fractional amplitude of the composited lower-
528 tropospheric $[Z]'$ relative to the upper-tropospheric eddies (Figs. 11d-f). In midwinter, the
529 relative amplitude of low-level anticyclonic eddies is indeed smaller than in the shoulder
530 seasons, which is consistent with Nakamura and Sampe (2002). The vertical connection
531 becomes more prominent in spring (Fig. 11f). Midwinter weakening of the vertical linkage is
532 also found in the corresponding composites for cyclonic vortices in the JPS domain (not
533 shown).

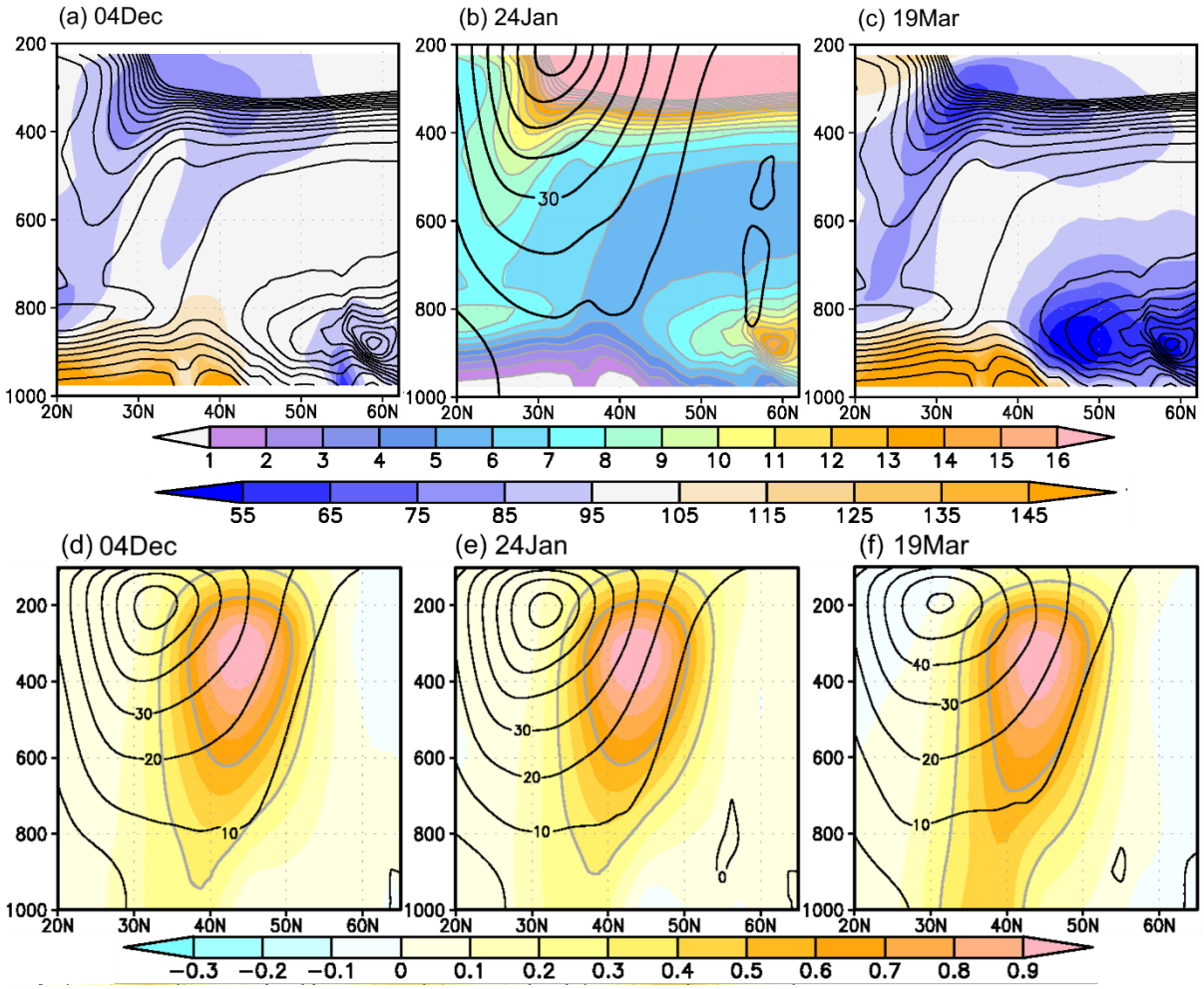


Fig. 11. (a) Ratio of climatological-mean vertical gradient of potential temperature for 04Dec to that for 24Jan (colors, %). Black contours are identical to grey contours in (b). (b) Meridional sections of the climatological-mean vertical gradient of potential temperature (colors, K/100hPa) and westerly wind speed (black contours, every 10m/s) for 24Jan. (c) Same as in (a), but for the climatological mean for 19Mar. All the quantities plotted have been averaged between 130°E and 140°E. (d-f) Meridional sections of composited high-pass-filtered anomalies of geopotential height normalized by the maximum value between the 500-hPa and 100-hPa levels (colors, m/m) at time steps when one or more anticyclonic centers are located over the Japan Sea domain for the calendar days as indicated. Values of 0.3 and 0.6 m/m are highlighted by grey contours. Black contours indicate climatological-mean westerly wind speed (every 10m/s). All the quantities plotted have been averaged between 125°E and 135°E.

## 5. Long-term modulations of the MWM

In this section, we briefly describe long-term modulations of densities of cyclone and anticyclone centers and associated background states. Following Nakamura et al. (2002), we divide the full analysis period into the earlier (1958/59−1985/86) and later (1986/87−2016/17) periods. The earlier (later) period is characterized by a stronger (weaker)

suppression of the midwinter NP storm-track activity. Note that results for the long-term modulations of frequency of surface cyclones/anticyclones are qualitatively the same when the latter period is extended to 2020/21.

The two periods are marked basically by the midwinter maximum in cyclone density and the MWM in anticyclonic density over the western NP (Fig. 12) as seen for the entire period, suggestive of robustness of the characteristics. Comparison between the two periods reveals, however, that the seasonality of cyclone and anticyclone densities shows long-term modulations. In the earlier period (Fig. 12a), southward expansion of the region of high cyclonic density persists longer than in the later period (Fig. 12c). In addition, in the earlier period (Fig. 12b), the MWM of anticyclonic density is more distinct, and its axis migrates further equatorward compared to the later period (Fig. 12d). It may be related to enhanced equatorward expansion of the AL as well as the southward-shifted and weakened subtropical high-pressure belt in midwinter in the earlier period (black contours in Fig. 12). This is consistent with the interdecadal modulations of the East Asian winter Monsoon shown by previous studies (Nakamura et al. 2002; Wang et al 2009).

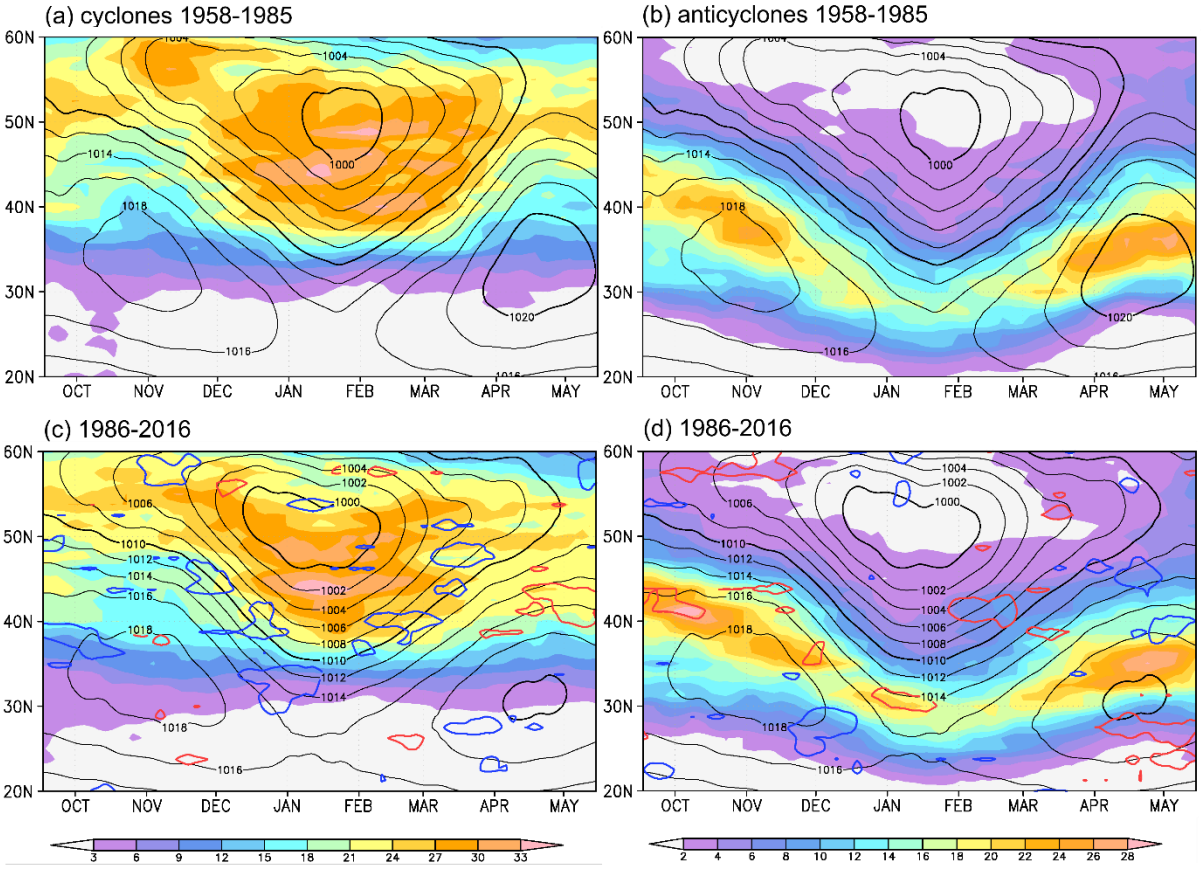

Fig. 12. Same as in Fig. 2, but for probability in (a-b) the earlier period (1958/59-1985/86) and (c-d) the later period (1986/87−2016/17). Red and blue contours in (c-d) denote statistically significant increase and decrease, respectively, from the former period at the 90% confidence level by Student's *t*-test.

The interpretation presented in the preceding section can also apply to the long-term modulations of anticyclonic density. Figures 13a and 13d show the density of surface anticyclones over the NP that have passed through the JPS domain as in section 4. Evidently, the contribution of anticyclones coming from the JPS domain to the MWM of the NP anticyclone density is more distinct during the earlier period than in the later. Though less significant, residual anticyclones increased in the later period, which also contributed to the weakening of the MWM in the total density over the NP (Figs. 13b and 13e). Conversely, the seasonal evolution of the density of residual cyclones over the NP is similar to that of the total density (Figs. 12 and 13), which is consistent with the results for the entire period. This result suggests that cyclones passing through the JPS domain may not be quite relevant to shaping the midwinter maximum of the NP cyclone density.

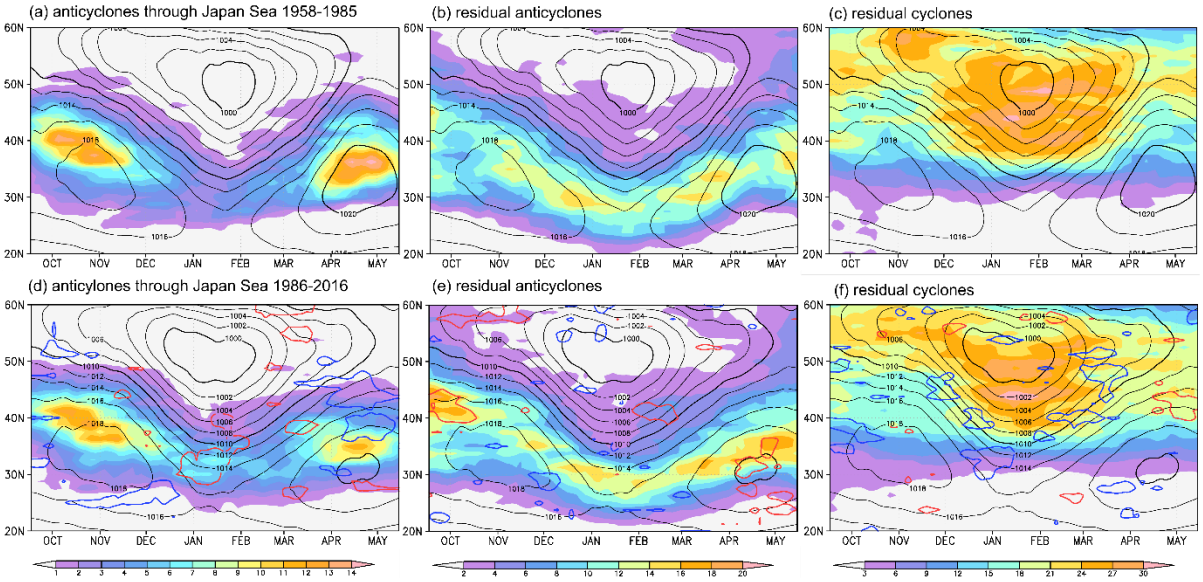


Fig. 13. (a-c) Same as in Figs. 5b, 5d and 5c, respectively, but for probability in the earlier period (1958/59−1985/86). (d-f) Same as in (a-c), respectively, but for probability in the later period (1986/87−2016/17). Red and blue contours in (d-f) denote statistically significant increase and decrease, respectively, from the former period at the 90% confidence level by Student's *t*-test.

In the later period, the wintertime NP upper-tropospheric westerly jet has widened poleward compared to the earlier period over the East Asian sector (Figs. 14a-c), which is

consistent with previous studies (e.g., Archer and Caldeira 2008). Though not statistically significant, the widening in the mid- and upper troposphere is most prominent in midwinter, while lower-tropospheric westerly intensification to the north of ~40°N is comparable between midwinter and early spring. Compared to the shoulder seasons, the corresponding long-term modulations of potential temperature are marked in midwinter with more rapid warming to the north (south) in the lower (upper) troposphere and the tropopause-level cooling especially to the north of 50°N (Figs. 14d-f). The warming in the lower- to mid-troposphere is statistically significant, especially in midwinter. It acts to attenuate the stratification just below the westerly jet axis (~600-300 hPa), leading to an increase in Rossby depth. In other words, the retardation of the vertical connection of upper-tropospheric eddies with near-surface disturbances in midwinter has been somewhat relaxed in the later period, which is consistent with the suggestion by Nakamura and Sampe (2002).

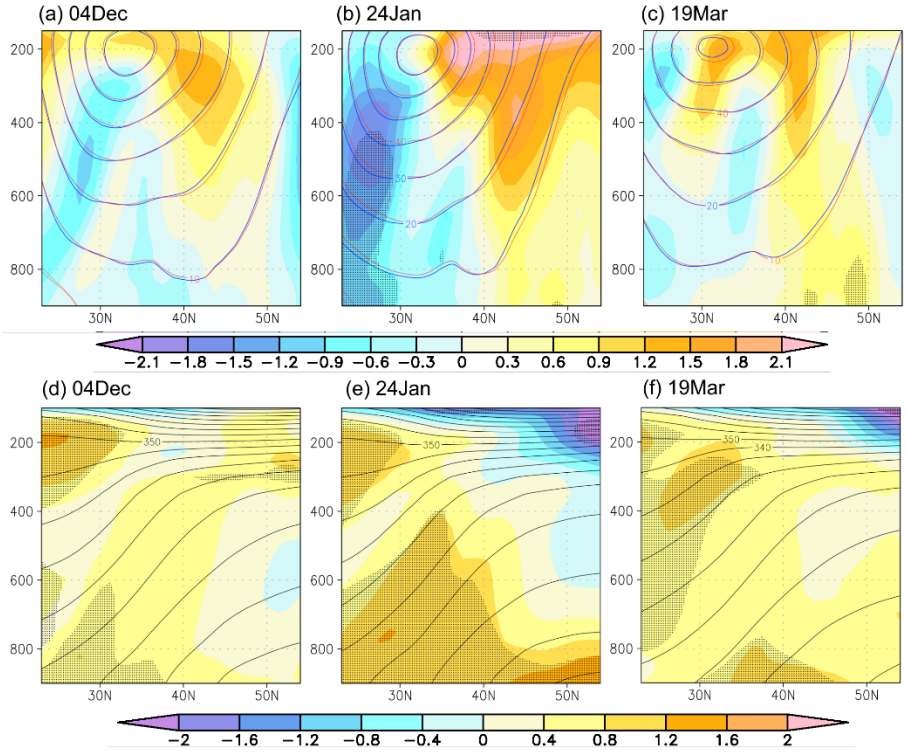


Fig. 14. (a-c) Differences in climatological-mean westerly wind speed (m/s; colored as indicated) averaged for 130°−140°E between the earlier (1958−1985) and later (1986−2016) periods. Blue and red contours denote climatological-mean westerly wind speed (m/s) in the earlier and later periods, respectively. Stippling indicates statistically significant difference at the 90% confidence level by Student's *t*-test. (d-f) Same as in (a-c), but for difference in climatological-mean potential temperature (K; colored as indicated). Black contours denote climatological-mean potential temperature (K) in the later period.

## 6. Summary and Discussions

In this study we investigate the detailed seasonal evolution of frequency of migratory surface anticyclone centers over the NP, in comparison with its cyclonic counterpart, based on the feature tracking algorithm described in section 2. We point out that the seasonality of those surface anticyclones is distinctively different from that of surface cyclones. Additionally, we revealed that the seasonality of the surface anticyclone density around the NP storm-track is substantially under the upstream influence, especially from the JPS domain located at the storm-track entrance region.

In the shoulder seasons, density of migratory surface anticyclones is relatively high over the JPS region under the frequent passage of upper-tropospheric anticyclonic vortices and relatively low mid-tropospheric static stability. Some of those anticyclones propagate into the NP storm-track region to form the two distinct peaks in the seasonal density of migratory anticyclones. In midwinter, on the contrary, density of surface anticyclones over JPS is lower under the less frequent passage of upper-tropospheric anticyclonic vortices and higher mid-tropospheric static stability in association with the monsoonal cold-air outbreaks and the excessively strong westerly jet-stream. In this circumstance, the vertical coupling between upper- and lower-tropospheric eddies tends to be retarded (Nakamura and Sampe 2002), leading to the distinct density minimum of migratory anticyclones over the NP. This is apparently inconsistent with the baroclinic instability theory.

The composite analysis for migratory anticyclones over the JPS domain indicates that they tend to be accompanied by persistent weakening of the climatological East Asian trough associated with upper-level planetary waves and associated lower-tropospheric warming. The weakening of the East Asian winter monsoon tends to be preceded by Rossby wave propagation from upstream. Midwinter anticyclones moving over the JPS domain are likely to be accompanied by stronger, more distinct low-frequency anomalies than in the shoulder seasons. This suggests that a more prominent, unusual weakening of the winter monsoon is needed for a migratory anticyclone over the JPS domain to form under the unfavorable climatological-mean condition, which is consistent with the fewer migratory anticyclones over the midwinter NP.

In sharp contrast to the seasonality of anticyclone density, density of migratory cyclones over the NP is maximized in midwinter, which is compatible with the baroclinic instability theory. It may be explained by local cyclogenesis around the Kamchatka Peninsula, Kuroshio

Extension, and East China Sea, rather than that over the JPS sector. Density of migratory surface cyclones over the JPS sector is indeed maximized under the more frequent upper-tropospheric cyclonic vortices aloft.

Additionally, we have briefly confirmed that the above discussion can be applied to interdecadal modulations of the MWM of the NP storm-track activity. In the more recent period after the mid-1980s, the MWM became less distinct both in the NP storm-track activity and NP anticyclone density, latter of which may be related to the less frequent anticyclones over JPS under the lowered mid-tropospheric static stability. In this period, the midwinter density of NP migratory cyclones became lower, although its midwinter maximum was still obvious.

The fact that anticyclones are less frequent over the midwinter NP in contrast to the midwinter maximum of cyclone density suggests that anticyclones may be the key to the understanding of the MWM of the NP storm-track activity, as measured by Eulerian eddy statistics (Nakamura 1992). Indeed, the anticyclonic contribution plays a pivotal role in setting the MWM of Eulerian eddy statistics such as $V'V'_{300}$ and $V'T'_{850}$ (Part II). As for its interdecadal modulations, both cyclones and anticyclones seem important for the sharpening of the midwinter maximum of cyclone density and the weakening of the MWM of anticyclonic density, respectively. In Part II, seasonal evolution of the contributions from cyclonic and anticyclonic vortices to Eulerian eddy statistics is also investigated.

The present study investigates densities of centers of migratory cyclones and anticyclones, which are influenced by both the number of tracks and their lifetime. We have compiled cyclone tracks passing the western NP domain [150°−180°E, 25°−55°N] in their lifetime. Compared to the shoulder seasons, the number of tracks increases in midwinter, which is found to dominate over the shortening of their typical lifetime and thus lead to the increase in density of NP cyclone centers as seen in Fig. 2. The result is qualitatively consistent with Schemm and Schneider (2018), and at least not contradicting the results for cyclones identified with 850-hPa vorticity by Hadas and Kaspi (2021), in a sense that the reduction in their lifetime is more distinct than that in their number. Note that their results are based on an aquaplanet GCM experiment with no land-sea contrast, unlike around the JPS domain. Interestingly, the midwinter decrease in the number of anticyclone tracks is also found to contribute to the MWM of the density of NP anticyclone centers on top of the shortening of their typical lifetime. Another aspect possibly relevant to this study is that

typical lifetime of cyclone tracks passing the JPS sector is not clearly suppressed in midwinter, while that of the corresponding anticyclones exhibits a distinct MWM. This may be interpreted as the different characteristics of vertical coupling between upper- and lower-tropospheric eddies for cyclones and anticyclones over the midwinter JPS. Specifically, surface cyclones are more likely to be coupled with upper-level cyclonic vortices under the moderate background westerly wind speed a little away from the jet axis after their northeastward propagation into the NP (Fig. 1). By contrast, migratory anticyclones are less likely to form, because frequency of upper-level anticyclonic vortices is climatologically reduced, and excessively strong background westerlies hamper the vertical coupling around the jet axis (Nakamura and Sampe 2002), owing to their southeastward propagation.

The composite analysis associated with JPS migratory anticyclones suggests their close relation to the EU teleconnection pattern. It has been suggested that the EU pattern exerts an influence onto the activity of the East Asian winter monsoon (Wang and Zhang 2005; Takaya and Nakamura 2013). The strength of the East Asian winter monsoon and upper-level East Asian trough is also closely related also to the western Pacific (WP)-like pattern (Takaya and Nakamura 2013; Wang and Chen 2014; Song et al. 2016). Compared to those previous studies, the anomalous low-frequency circulation typically associated with a JPS anticyclone is characterized more by Rossby wave propagation over Eurasia rather than a WP-like anomaly (Fig. 9). It has been suggested that the EU pattern is linked more to North Atlantic SST anomalies, while WP-like pattern tends to be under the remote influences of the ENSO variability (Takaya and Nakamura 2013) and the variability of the Australian summer monsoon (Sekizawa et al. 2021). Additionally, the influence of Arctic sea ice, especially over the Brents-Kara Sea, on the East Asian winter monsoon has been recently intensively investigated. Some of those studies suggested that Arctic sea ice loss, which has become distinct after 2000s, tends to be linked with the blocking formation around the Ural region and the stronger East Asian trough (e.g., Kim et al. 2014; Mori et al. 2014, 2019; Zhang et al. 2018; Tyrlis et al. 2020). Zhang et al. (2022) suggested that the interdecadal change in EAWM around the 2000s is related to the recent Arctic sea ice loss. Potential influence from those external forcing onto the activity of JPS anticyclones and the MWM of the NP storm-track activity is in our future scope.

Considering that the midwinter suppression of storm-track activity is a unique phenomenon for the NP, comparison of the seasonality in cyclone and anticyclone densities

between the NP and NA storm-tracks is also needed. In fact, our preliminary result indicates that the seasonality in cyclonic and anticyclonic densities over the NA is not as discernible as over the NP (not shown). The brief investigation of the long-term modulations of the MWM of the NP storm-track activity in this study should be complemented by a more detailed study in future. Interannual variability of the storm-track activity is also to be examined.

*Acknowledgments.*

This study is supported in part by the Japanese Ministry of Education, Culture, Sports, Science and Technology (MEXT) through the Arctic Challenge for Sustainability (ArCS-II), by the Japan Science and Technology Agency through COI-NEXT JPMJPF2013, by the Environmental Restoration and Conservation Agency of Japan through Environment Research and Technology Development Fund JPMEERF20222002, and by the Japan Society for the Promotion of Science (JSPS) through Grants-in-Aid for Scientific Research 19H05702 (on Innovative Areas 6102), 20H01970, 22H01292 and 22K14097. It is also supported by JSPS-ISF Joint Research Project (JPJSBP120218403). Y.K. acknowledges support from the JSPS Invitational Fellowship for Research in Japan that supported a sabbatical at the University of Tokyo and ignited this collaboration, for support from the Research Center for Advanced Technology and Science at the University of Tokyo and the Israeli Science Foundation (grant 996/20).

*Data Availability Statement.*

The JRA-55 atmospheric reanalysis is available online from the Japan Meteorological Agency at https://jra.kishou.go.jp/JRA-55/index_en.html as cited in Kobayashi et al. (2015) and Harada et al. (2016). The d4PDF is available at http://www.miroc-gcm.jp/~pub/d4PDF/index_en.html.

## APPENDIX

### Appendix. Assessment of feature tracking algorithm

In this study, tracks of surface centers of migratory cyclones and anticyclones are objectively identified by the procedure described in section 2. It is established that

identification of cyclone tracks can be influenced by a tracking scheme used (Ulbrich et al. 2009). Therefore, given the identification algorithm used in this study includes some degree of arbitrariness, it is important to assess the performance of the tracking algorithm.

As the most intuitive way, we have verified identified cyclone and anticyclone centers in snapshots. As mentioned in section 2, the procedure has been constructed to identify features as migratory synoptic-scale cyclones and anticyclones represented on a surface weather map. Indeed, identified centers are consistent with a SLP field as a given snapshot in Fig. A1a.

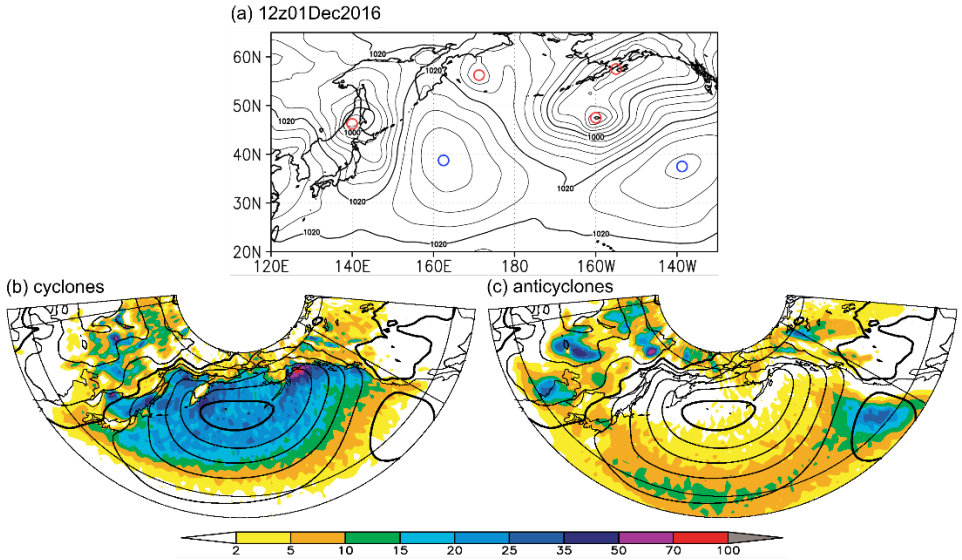


Fig. A1. (a) Snapshot of SLP (black contours, every 4hPa) and identified cyclone and anticyclone centers (red and blue open circles, respectively) at 1200UTC01Dec2016. (b) Wintertime (DJF) climatological-mean density of identified surface cyclone centers (%/(1000km)$^2$) based on the JRA-55 for 1958/59−2016/17. Unit is set to be the same in Neu et al. (2013). Meridians of 100°E and 120°W are highlighted, which indicate the western and eastern boundaries of the domain through which the identified centers must pass. (c) Same as in (b), but for identified anticyclone centers.

It is also of particular importance to compare our tracking results with those in previous studies. The wintertime (DJF) cyclone density with our tracking algorithm is clearly within a range of variations among those algorithms in the IMILAST project (Neu et al. 2013) in its overall density values and horizontal distribution. It is noteworthy that the cyclone density with our algorithm is consistent especially with that with algorithms using both SLP and $\nabla^2$SLP (or, equivalently, surface vorticity). Meanwhile, the anticyclonic density has much fewer literature to be compared with. Nevertheless, our result is qualitatively consistent with the results by Hoskins and Hodges (2002) and Pepler et al. (2019). One discernible characteristic of our result compared with the previous studies, especially Hoskins and

Hodges (2002), is a density maximum over the eastern NP collocated with the climatological center of the southeastward-retreated wintertime subtropical high. The difference is presumably caused by the different ways of calculating density from track data to draw spatial maps. That is, while Hoskins and Hodges (2002) computed density using all grid points along a given track, the present study assembles grid points at which an anticyclone center exists in a particular time step. The difference should lead to lower (higher) density over domains where a typical propagation speed of anticyclones is fast (slow) compared to Hoskins and Hodges (2002), which can be evidently seen in Fig. A1c. We confirm that the density maximum over the eastern NP becomes less distinct when all grid points along a track are taken into account (not shown). Nevertheless, the density of centers of features is comparable more directly with results for Eulerian eddy statistics (Okajima et al. 2022a), which is the central purpose of Part II.

## REFERENCES


Afargan, H., and Y. Kaspi, 2017: A midwinter minimum in North Atlantic storm track intensity in years of a strong jet. Geophys. Res. Lett., 44(24), 12–511.

Archer, C. L., and K. Caldeira, 2008: Historical trends in the jet streams. Geophys. Res. Lett., 35(8).

Battalio, J. M., 2022: Transient eddy kinetic energetics on Mars in three reanalysis datasets. J. Atmos. Sci., 79(2), 361-382.

Bell, G. D., and L. F. Bosart, 1989: A 15-year climatology of Northern Hemisphere 500 mb closed cyclone and anticyclone centers. Mon. Wea. Rev., 117(10), 2142-2164.

Blackmon, M. L., 1976: A climatological spectral study of the 500 mb geopotential height of the Northern Hemisphere. J. Atmos. Sci., 33(8), 1607–1623.

Blackmon, M. L., J. M. Wallace, N. C. Lau, and S. L. Mullen, 1977: An observational study of the Northern Hemisphere wintertime circulation. J. Atmos. Sci., 34(7), 1040–1053.

Blackmon, M. L., Y. H. Lee, and J. M. Wallace, 1984: Horizontal structure of 500 mb height fluctuations with long, intermediate and short time scales. J. Atmos. Sci., 41(6), 961-980.

Bueh, C., and H. Nakamura, 2007: Scandinavian pattern and its climatic impact. Quart. J. Roy. Meteor. Soc., 133, 2117–2131.

796 Catto, J. L., L. C. Shaffrey, and K. I. Hodges, 2010: Can climate models capture the structure
797 of extratropical cyclones? J. Climate, 23(7), 1621-1635.

798 Chang, E. K., 2001: GCM and observational diagnoses of the seasonal and interannual
799 variations of the Pacific storm track during the cool season. J. Atmos. Sci., 58(13), 1784–
800 1800.

801 Chang, E. K., S. Lee, and K. L. Swanson, 2002: Storm track dynamics. J. Climate, 15(16),
802 2163–2183.

803 Chang, E. K., 2005: The impact of wave packets propagating across Asia on Pacific cyclone
804 development. Mon. Wea. Rev., 133(7), 1998-2015.

805 Chang, E. K., and S. Song, 2006: The seasonal cycles in the distribution of precipitation
806 around cyclones in the western North Pacific and Atlantic. J. Atmos. Sci., 63(3), 815–
807 839.

808 Chang, E. K., and Y. Guo, 2012: Is Pacific storm-track activity correlated with the strength of
809 upstream wave seeding?, J. Climate, 25(17), 5768–5776.

810 Christoph, M., U. Ulbrich, and P. Speth, 1997: Midwinter suppression of Northern
811 Hemisphere storm track activity in the real atmosphere and in GCM experiments. J.
812 Atmos. Sci., 54(12), 1589-1599.

813 Deng, Y., and M. Mak, 2005: An idealized model study relevant to the dynamics of the
814 midwinter minimum of the Pacific storm track. J. Atmos. Sci., 62(4), 1209–1225.

815 Deng, Y., and M. Mak, 2006: Nature of the differences in the intraseasonal variability of the
816 Pacific and Atlantic storm tracks: A diagnostic study. J. Atmos. Sci., 63(10), 2602–2615.

817 Eady, E. T., 1949: Long waves and cyclone waves. Tellus, 1(3), 33–52.

818 Favre, A., and A. Gershunov, 2006: Extra-tropical cyclonic/anticyclonic activity in North-
819 Eastern Pacific and air temperature extremes in Western North America. Clim. Dyn.,
820 26(6), 617-629.

821 Frierson, D. M. W., and N. A. Davis, 2011: The seasonal cycle of midlatitude static stability
822 over land and ocean in global reanalyses. Geophys. Res. Lett., 38(13).

823 Hadas, O., and Y. Kaspi, 2021: Suppression of baroclinic eddies by strong jets. J. Atmos.
824 Sci., 78(8), 2445-2457.

825 Harada, Y., H. Kamahori, C. Kobayashi, H. Endo, S. Kobayashi, Y. Ota, H. Onoda, K.
826 Onogi, K. Miyaoka, and K. Takahashi, 2016: The JRA-55 Reanalysis: Representation of
827 atmospheric circulation and climate variability, J. Meteor. Soc. Japan, 94, 269–302.

828 Harnik, N., and E. K. Chang, 2004: The effects of variations in jet width on the growth of
829 baroclinic waves: Implications for midwinter Pacific storm track variability. J. Atmos.
830 Sci., 61(1), 23–40.

831 Hewson, T. D., and H. A. Titley, 2010: Objective identification, typing and tracking of the
832 complete life-cycles of cyclonic features at high spatial resolution. Meteor. Appl., 17(3),
833 355-381.

834 Hinman, R., 1888: Eclectic physical geography. American Book Company.

835 Hodges, K. I., 1994: A general method for tracking analysis and its application to
836 meteorological data. Mon. Wea. Rev., 122(11), 2573-2586.

837 Hodges, K. I., 1995: Feature tracking on the unit sphere. Mon. Wea. Rev., 123(12), 3458-
838 3465.

839 Hoskins, B. J., and K. I. Hodges, 2002: New perspectives on the Northern Hemisphere winter
840 storm tracks. J. Atmos. Sci., 59(6), 1041-1061.

841 Hoskins, B. J., and K. I. Hodges, 2019a: The annual cycle of Northern Hemisphere storm
842 tracks. Part I: Seasons. J. Climate, 32(6), 1743-1760.

843 Hoskins, B. J., and K. I. Hodges, 2019b: The annual cycle of Northern Hemisphere storm
844 tracks. Part II: Regional detail. J. Climate, 32(6), 1761-1775.

845 Ioannidou, L., and M. K. Yau, 2008: A climatology of the Northern Hemisphere winter
846 anticyclones. J. Geophys. Res. Atmos., 113(D8).

847 James, I. N., 1987: Suppression of baroclinic instability in horizontally sheared flows. J.
848 Atmos. Sci., 44(24), 3710–3720.

849 Kim, B., and coauthors, 2014: Weakening of the stratospheric polar vortex by Arctic sea-ice
850 loss. Nat. Comm., 5(1), 1-8.

851 Klein, W. H., 1958: The frequency of cyclones and anticyclones in relation to the mean
852 circulation. Journal of Meteorology, 15(1), 98-102.

853 Kobayashi, S., Y. Ota, Y. Harada, A. Ebita, M. Moriya, H. Onoda, K. Onogi, H. Kamahori,
854 C. Kobayashi, H. Endo, K. Miyaoka, and K. Takahashi, 2015: The JRA-55 Reanalysis:
855 General specifications and basic characteristics. J. Meteor. Soc. Japan, 93, 5–48.

856 Kravtsov, S., I. Rudeva, and S. K. Gulev, 2015: Reconstructing sea level pressure variability
857 via a feature tracking approach. J. Atmos. Sci., 72(1), 487-506.

858 Kuwano-Yoshida, A., S. Okajima, and H. Nakamura, 2021: Rapid increase of explosive
859 cyclone activity over the midwinter North Pacific in the late 1980s. J. Climate, 35(3),
860 1113-1133.

861 Lachmy, O., and N. Harnik, 2014: The transition to a subtropical jet regime and its
862 maintenance. J. Atmos. Sci., 71(4), 1389–1409.

863 Lachmy, O., and N. Harnik, 2016: Wave and jet maintenance in different flow regimes. J.
864 Atmos. Sci., 73(6), 2465–2484.

865 Lee, S. S., J. Y. Lee, K. J. Ha, B. Wang, A. Kitoh, Y. Kajikawa, and M. Abe, 2013: Role of
866 the Tibetan Plateau on the annual variation of mean atmospheric circulation and storm-
867 track activity. J. Climate, 26(14), 5270–5286.

868 Lewis, S. R., D. P. Mulholland, P. L. Read, L. Montabone, R. J. Wilson, and M. D. Smith,
869 2016: The solsticial pause on Mars: 1. A planetary wave reanalysis. *Icarus*, 264, 456-464.

870 Lorenz, E. N., 1955: Available potential energy and the maintenance of the general
871 circulation. Tellus, 7(2), 157-167.

872 Manobianco, J., 1989: Explosive east coast cyclogenesis over the west-central North Atlantic
873 Ocean: A composite study derived from ECMWF operational analyses. Mon. Wea. Rev.,
874 117(11), 2365-2383.

875 Masunaga, R., H. Nakamura, B. Taguchi, and T. Miyasaka, 2020: Processes Shaping the
876 Frontal-Scale Time-Mean Surface Wind Convergence Patterns around the Kuroshio
877 Extension in Winter. J. Climate, 33(1), 3-25.

878 Mori, M., M. Watanabe, H. Shiogama, J. Inoue, and M. Kimoto, 2014: Robust Arctic sea-ice
879 influence on the frequent Eurasian cold winters in past decades. Nat. Geosci., 7(12), 869-
880 873.

881 Mori, M., Y. Kosaka, M. Watanabe, H. Nakamura, and M. Kimoto, 2019: A reconciled
882 estimate of the influence of Arctic sea-ice loss on recent Eurasian cooling. Nat. Clim.
883 Change, 9(2), 123-129.

884 Murray, R. J., and I. Simmonds, 1991: A numerical scheme for tracking cyclone centres from
885 digital data. Aust. Meteor. Mag., 39(3), 155-166.

886 Nakamura, H., 1992: Midwinter suppression of baroclinic wave activity in the Pacific. J.
887 Atmos. Sci., 49(17), 1629–1642.

888 Nakamura, H., and T. Sampe, 2002: Trapping of synoptic-scale disturbances into the North-
889 Pacific subtropical jet core in midwinter. Geophys. Res. Lett., 29(16), 2228.

890 Nakamura, H., T. Izumi, and T. Sampe, 2002: Interannual and decadal modulations recently
891 observed in the Pacific storm track activity and East Asian winter monsoon. J. Climate,
892 15(14), 1855–1874.

893 Nakamura, H., T. Sampe, Y. Tanimoto, and A. Shimpo, 2004: Observed associations among
894 storm tracks, jet streams, and midlatitude oceanic fronts. Earth Climate: The Ocean–
895 Atmosphere Interaction, Geophys. Monogr., 147, Amer. Geophys. Union, 329–345.

896 Nakamura, H., T. Miyasaka, Y. Kosaka, K. Takaya, K., and M. Honda, 2010: Northern
897 Hemisphere extratropical tropospheric planetary waves and their low-frequency
898 variability: Their vertical structure and interaction with transient eddies and surface
899 thermal contrasts. Climate dynamics: why does climate vary, 189, 149-179.

900 Nakamura, N., 1988: Scale selection of baroclinic instability – Effects of stratification and
901 nongeostrophy. J. Atmos. Sci., 45(21), 3253-3268.

902 Neu, U., and coauthors, 2013: IMILAST: A community effort to intercompare extratropical
903 cyclone detection and tracking algorithms. Bull. Amer. Meteor. Soc., 94(4), 529-547.

904 Novak, L., T. Schneider, and F. Ait-Chaalal, 2020: Midwinter suppression of storm tracks in
905 an idealized zonally symmetric setting. J. Atmos. Sci., 77(1), 297–313.

906 Okajima, S., H. Nakamura, and Y. Kaspi, 2021: Cyclonic and anticyclonic contributions to
907 atmospheric energetics. Sci. Rep., 11(1), 1-10.

908 Okajima, S., H. Nakamura, and Y. Kaspi, 2022a: Energetics of transient eddies related to the
909 midwinter minimum of the North Pacific storm-track activity. J. Climate., 35(4), 1137-
910 1156.

911 Okajima, S., H. Nakamura, and Y. Kaspi, 2022b: Distinct roles of cyclones and anticyclones
912 in setting the midwinter minimum of the North Pacific eddy activity. Part II: Eulerian
913 eddy statistics and energetics. J. Climate, submitted.

914 Park, H. S., J. C. Chiang, and S. W. Son, 2010: The role of the central Asian mountains on
915 the midwinter suppression of North Pacific storminess. J. Atmos. Sci., 67(11), 3706–
916 3720.

917 Parker, S. S., J. T. Hawes, S. J. Colucci, and B. P. Hayden, 1989: Climatology of 500 mb
918 cyclones and anticyclones, 1950–85. Mon. Wea. Rev., 117(3), 558-571.

919 Penny, S., G. H. Roe, and D. S. Battisti, 2010: The source of the midwinter suppression in
920 storminess over the North Pacific. J. Climate, 23(3), 634–648.

921 Pepler, A., A. Dowdy, and P. Hope, 2019: A global climatology of surface anticyclones, their
922 variability, associated drivers and long-term trends. Clim. Dyn., 52(9), 5397-5412.

923 Pinto, J. G., T. Spangehl, U. Ulbrich, and P. Speth, 2005: Sensitivities of a cyclone detection
924 and tracking algorithm: individual tracks and climatology. Meteorol. Z., 14(6), 823-838.

925 Sawyer, J. S., 1970: Observational characteristics of atmospheric fluctuations with a time
926 scale of a month. Q. J. Royal Meteorological Soc., 96(410), 610-625.

927 Schemm, S. and T. Schneider, 2018: Eddy lifetime, number, and diffusivity and the
928 suppression of eddy kinetic energy in midwinter. J. Climate, 31(14), 5649-5665.

929 Schemm, S., and G. Rivière, 2019. On the Efficiency of Baroclinic Eddy Growth and how it
930 Reduces the North Pacific Storm Track Intensity in Midwinter. J. Climate, 32(23), 8373–
931 8398.

932 Schemm, S., H. Wernli, and H. Binder, 2021: The storm-track suppression over the western
933 North Pacific from a cyclone life-cycle perspective, Wea. Clim. Dyn., 2, 55-69.

934 Sekizawa, S., H. Nakamura, and Y. Kosaka, 2021: Remote Influence of the Interannual
935 Variability of the Australian Summer Monsoon on Wintertime Climate in East Asia and
936 the Western North Pacific. J. Climate, 34(23), 9551-9570.

937 Shaw, T. A., M. Baldwin, E. A. Barnes, R. Caballero, C. I. Garfinkel, Y.-T. Hwang, C. Li, P.
938 A. O'Gorman, G. Riviere, I. Simpson, and A. Voigt, 2016: Storm track processes and the
939 opposing influences of climate change. Nat. Geosci., 9, 656–664.

940 Simmonds, I., C. Burke, and K. Keay, 2008: Arctic climate change as manifest in cyclone
941 behavior. J. Climate, 21(22), 5777-5796.

942 Song, L., L. Wang, W. Chen, and Y. Zhang, 2016: Intraseasonal variation of the strength of
943 the East Asian trough and its climatic impacts in boreal winter. J. Climate, 29(7), 2557-
944 2577.

945 Takano, I., 2002: Analysis of an intense winter extratropical cyclone that advanced along the
946 south coast of Japan. J. Meteor. Soc. Japan, 80(4), 669-695.

947 Takaya, K., and H. Nakamura, 2001: A formulation of a phase-independent wave-activity
948 flux for stationary and migratory quasigeostrophic eddies on a zonally varying basic flow.
949 J. Atmos. Sci., 58, 608–627.

950 Takaya, K., and H. Nakamura, 2005: Geographical dependence of upper-level blocking
951 formation associated with intraseasonal amplification of the Siberian high. J. Atmos. Sci.,
952 62(12), 4441-4449.

953 Takaya, K., and H. Nakamura, 2013: Interannual variability of the East Asian winter
954 monsoon and related modulations of the planetary waves. J. Climate, 26(23), 9445-9461.

955 Takayabu, I., 1991: "Coupling development": an efficient mechanism for the development of
956 extratropical cyclones. J. Meteor. Soc. Japan, 69(6), 609-628.

957 Tamarin, T., and Y. Kaspi, 2016: The poleward motion of extratropical cyclones from a
958 potential vorticity tendency analysis. J. Atmos. Sci., 73(4), 1687-1707.

959 Tyrlis, E., J. Bader, E. Manzini, J. Ukita, H. Nakamura, and D. Matei, 2020: On the role of
960 Ural Blocking in driving the Warm Arctic–Cold Siberia pattern. Quart. J. Roy. Meteor.
961 Soc., 146(730), 2138-2153.

962 Ulbrich, U., G. C. Leckebusch, and J. G. Pinto, 2009: Extra-tropical cyclones in the present
963 and future climate: a review. Theoretical and Applied Climatology, 96(1-2), 117-131.

964 Wallace, J. M., and D. S. Gutzler, 1981: Teleconnections in the geopotential height field
965 during the Northern Hemisphere winter. Mon. Wea. Rev., 109(4), 784-812.

966 Wallace, J. M., G. H. Lim, and M. L. Blackmon, 1988: Relationship between cyclone tracks,
967 anticyclone tracks and baroclinic waveguides. J. Atmos. Sci., 45, 439–462.

968 Wang, C. C., and J. C. Rogers, 2001: A composite study of explosive cyclogenesis in
969 different sectors of the North Atlantic. Part I: Cyclone structure and evolution. Mon. Wea.
970 Rev., 129(6), 1481-1499.

971 Wang, L., R. Huang, L. Gu, W. Chen, and L. Kang, 2009: Interdecadal variations of the East
972 Asian winter monsoon and their association with quasi-stationary planetary wave activity.
973 J. Climate, 22(18), 4860-4872.

974 Wang, L., and W. Chen, 2014: An intensity index for the East Asian winter monsoon. J.
975 Climate, 27(6), 2361-2374.

976 Wang, N., and Y. Zhang, 2015: Evolution of Eurasian teleconnection pattern and its
977 relationship to climate anomalies in China. Clim. Dyn., 44(3-4), 1017-1028.

978 Watanabe, S. I., H. Niino, and W. Yanase, 2018: Composite analysis of polar mesocyclones
979 over the western part of the Sea of Japan. Mon. Wea. Rev., 146(4), 985-1004.

980 Whittaker, L. M., and L. H. Horn, 1984: Northern Hemisphere extratropical cyclone activity
981 for four mid-season months. Journal of Climatology, 4(3), 297-310.

982 Whitaker, J. S., and P. D. Sardeshmukh, 1998: A linear theory of extratropical synoptic eddy
983 statistics. J. Atmos. Sci., 55(2), 237–258.

984 Yanase, W., H. Niino, I. W. Shun-ichi, K. Hodges, M. Zahn, T. Spengler, and I. A. Gurvich,
985 2016: Climatology of polar lows over the Sea of Japan using the JRA-55 reanalysis. J.
986 Climate, 29(2), 419-437.

987 Yang, M., C. Li, X. Chen, Y. Tan, X. Li, C. Zhang, and G. Chen, 2021: The Climatology and
988 the Midwinter Suppression of the Cold-Season North Pacific Storm Track in CMIP6
989 Models. J. Climate, 34(17), 6971-6988.

990 Yuval, J., and Y. Kaspi, 2018: Eddy sensitivity to jet characteristics. J. Atmos. Sci., 75(5),
991 1371–1383.

992 Yuval, J., H. Afargan, and Y. Kaspi, 2018: The relation between the seasonal changes in jet
993 characteristics and the Pacific Midwinter Minimum in eddy activity. Geophys. Res. Lett.,
994 45(18), 9995–10002.

995 Zhao, Y., and X. S. Liang, 2019: Causes and underlying dynamic processes of the mid-winter
996 suppression in the North Pacific storm track. Sci. China Earth Sci., 62(5), 872–890.

997 Zhang, Y., K. R. Sperber, and J. S. Boyle, 1997: Climatology and interannual variation of the
998 East Asian winter monsoon: Results from the 1979–95 NCEP/NCAR reanalysis. Mon.
999 Wea. Rev., 125(10), 2605-2619.

1000 Zhang, Y., and I. M. Held, 1999: A linear stochastic model of a GCM's midlatitude storm
1001 tracks. J. Atmos. Sci., 56(19), 3416–3435.

1002 Zhang, P., Y. Wu, I. R. Simpson, K. L. Smith, X. Zhang, B. De, and P. Callaghan, 2018: A
1003 stratospheric pathway linking a colder Siberia to Barents-Kara Sea ice loss. Science
1004 advances, 4(7), eaat6025.

1005 Zhang, R., R. Zhang, and C. Sun, 2022: Modulation of the interdecadal variation of
1006 atmospheric background flow on the recent recovery of the EAWM during the 2000s and
1007 its link with North Atlantic–Arctic warming. *Clim. Dyn.*, 1-18.
1008

# Supplementary Materials

## 1. Tracking results with d4PDF

In this study, tracks of surface centers of moving cyclones and anticyclones are identified on the basis of the JRA-55 atmospheric reanalysis (Kobayashi et al. 2015) for a relatively long period (~60 years). The robustness of the seasonality of cyclone and anticyclone track densities based on the reanalysis is further verified by utilizing the Database for Policy Decision Making for Future Climate Change (d4PDF; Mizuta et al. 2017; Fujita et al. 2019). The d4PDF has been developed with the Meteorological Research Institute Atmospheric General Circulation Model (MRI-AGCM) version 3.2, whose horizontal resolution is TL319 (equivalent to ~60 km grid) with 64 vertical levels (up to 0.01 hPa). To minimize the effect of difference in horizontal resolutions, SLP fields have been interpolated onto a 1.25°×1.25° grid before identifying cyclone and anticyclone tracks. We take full advantage of 100-member historical simulations for 1958–2011.

The climatological-mean cyclone and anticyclone track densities are shown in Fig. S1. Evidently, the horizontal distributions of track densities are consistent with those based on the JRA-55 (Fig. 1), indicative of their high robustness. The consistency of the seasonality of the NP cyclone and anticyclone densities can be further confirmed in latitude-season sections similar to Fig. 2. As shown in Fig. S2, the distinctive seasonality between surface cyclone and anticyclone densities is consistent with our result with the JRA-55. The two peaks of the NP anticyclone density in the shoulder seasons are explained by anticyclones from the upstream, whereas cyclones from JPS exert only weak influence on the NP cyclone density compared to the residual. There are some minor differences in the results between the two datasets, including a peak (at ~45°N) of cyclonic density from JPS in early winter and slight increase of midwinter residual anticyclonic density. Nevertheless, the importance of anticyclones passing JPS for the seasonality of anticyclone density over the NP is thus verified with the large-ensemble climate model output covering nearly 6,000 cold seasons.

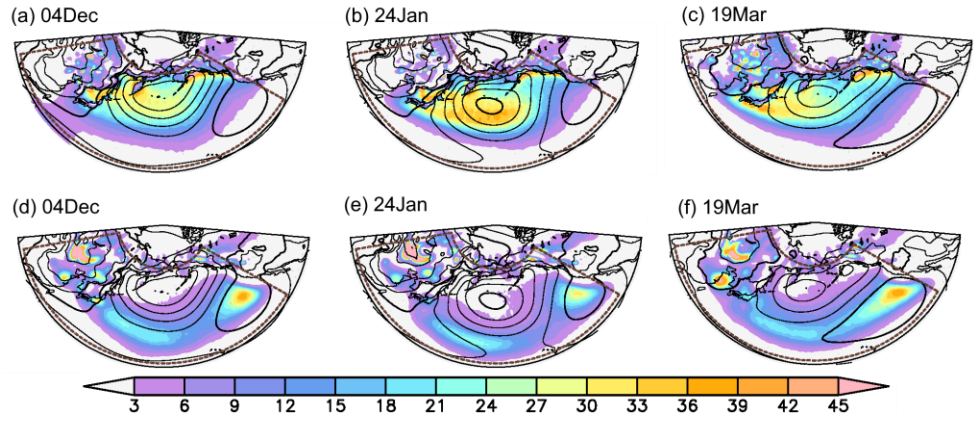


1035

1036 Fig. S1. Same as in Fig. 1, but for ensemble-mean probability based on 100 members of
1037 the d4PDF historical simulation for 1951-2010.

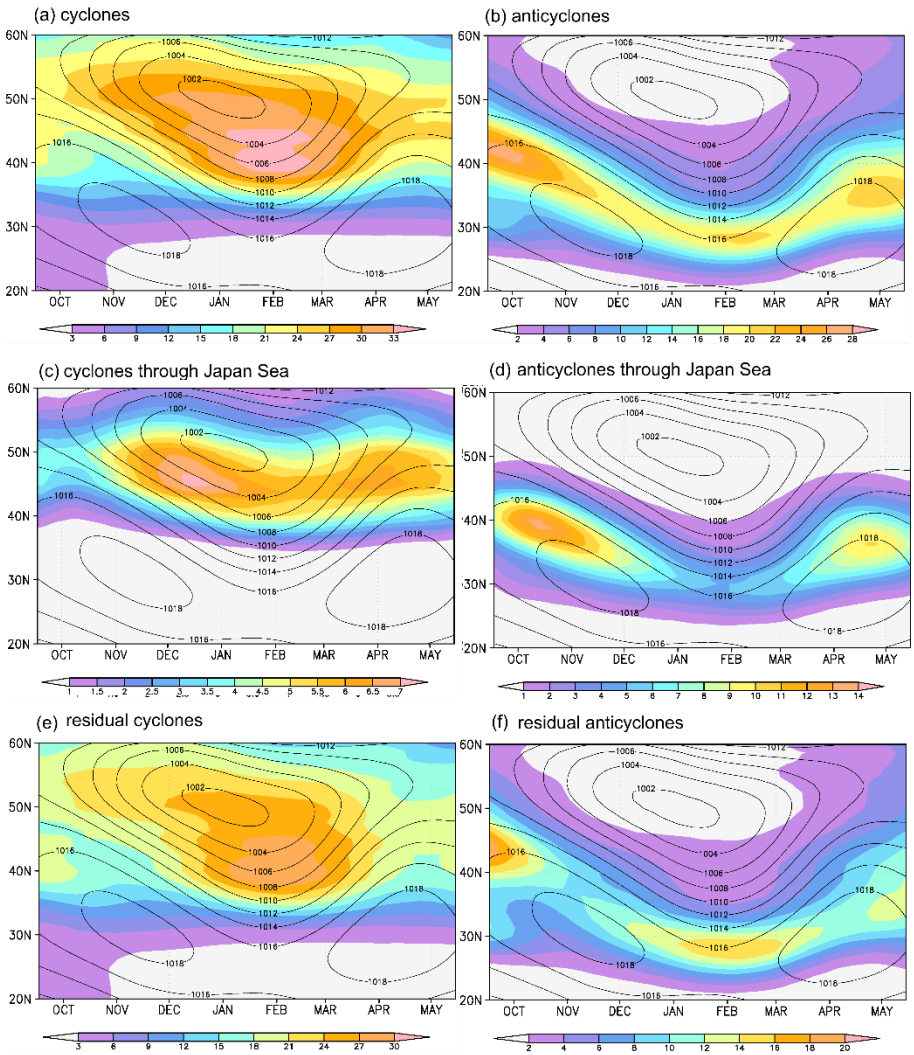


1038

1039 Fig. S2. (a, b) Same as in Figs. 2a-b, respectively, but for ensemble-mean probability
1040 based on 100 members of the d4PDF historical simulation for 1951-2010. (c-f) Same as in
1041 Figs. 5a-d, respectively, bur for ensemble-mean probability based on 100 members of d4PDF
1042 historical simulation for 1951-2010.

1043

## 2. Tracking of upper-tropospheric vortices

To further confirm the seasonality of the frequency of upper-tropospheric cyclonic and anticyclonic eddies, the seasonal march of climatological-mean density of centers of migratory cyclonic and anticyclonic vortices at 300 hPa is investigated. To identify tracks of vortex centers, we apply the same tracking procedure to a curvature field as used for migratory surface anticyclones. After the curvature has been horizontally smoothed with the 9-point horizontal smoothing performed six times, only a curvature maximum (minimum) that is highest (lowest) within an 800km circle around the extremum was identified as the center of the 300-hPa cyclonic (anticyclonic) vortex. The nearest curvature extremum identified above at successive time steps were connected. The distance must not exceed 1200km. As migratory surface features, any track must persist at least over 4 time steps (i.e., 24 hours) and travel at least over 600km during the lifetime.

Figure S3 shows the seasonal march of frequency of upper-tropospheric migratory cyclonic and anticyclonic vortices. The result is overall similar to Fig. 6 for their surface counterpart, indicating that the frequency of upper-tropospheric vortices identified only with local curvature appears to capture the characteristic seasonality of upper-level migratory eddies, especially for vortices observed north of ~42°N, although the detection procedure includes some arbitrariness in the choice of parameters. Note that the frequency of 'centers' of troughs or ridges is shown here, which are likely to be located north of the JPS domain.

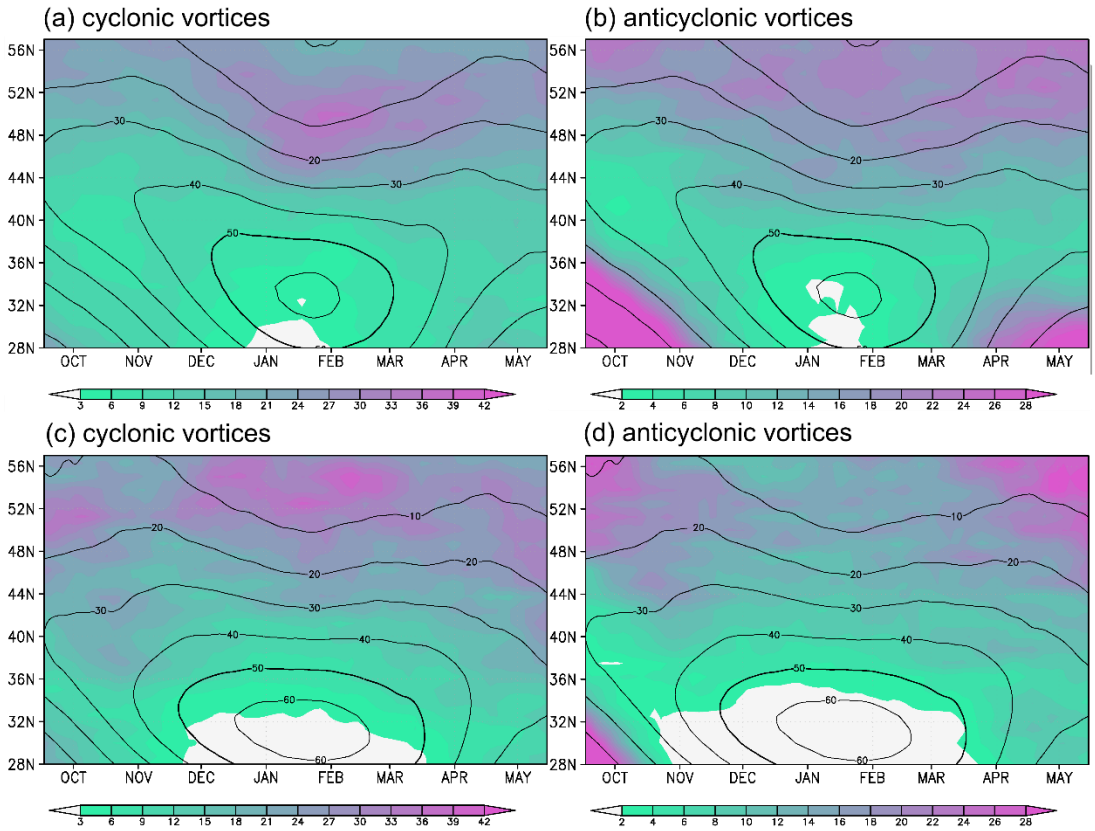


Fig. S3. Same as in Fig. 6, but for climatological-mean density (colors, *0.01%) of centers of migratory (a, c) cyclonic and (b, d) anticyclonic vortices at 300-hPa.

## REFERENCES

Fujita, M., and coauthors, 2019: Precipitation changes in a climate with 2-K surface warming from large ensemble simulations using 60-km global and 20-km regional atmospheric models. Geophys. Res. Lett., 46(1), 435-442.

Mizuta, R., and coauthors, 2017: Over 5,000 years of ensemble future climate simulations by 60-km global and 20-km regional atmospheric models. Bull. Amer. Meteor. Soc., 98(7), 1383-1398.